

Variable Read Disturbance: An Experimental Analysis of Temporal Variation in DRAM Read Disturbance

Ataberk Olgun[†] F. Nisa Bostancı[†] İsmail Emir Yüksel[†] Oğuzhan Canpolat[†] Haocong Luo[†]
Geraldo F. Oliveira[†] A. Giray Yağlıkcı[†] Minesh Patel[‡] Onur Mutlu[†]

ETH Zurich[†] Rutgers University[‡]

Modern DRAM chips are subject to read disturbance errors. These errors manifest as security-critical bitflips in a victim DRAM row that is physically nearby a repeatedly activated (opened) aggressor row (RowHammer) or an aggressor row that is kept open for a long time (RowPress). State-of-the-art read disturbance mitigations rely on accurate and exhaustive characterization of the read disturbance threshold (RDT) (e.g., the number of aggressor row activations needed to induce the first RowHammer or RowPress bitflip) of every DRAM row (of which there are millions or billions in a modern system) to prevent read disturbance bitflips securely and with low overhead.

We experimentally demonstrate for the first time that the RDT of a DRAM row significantly and unpredictably changes over time. We call this new phenomenon variable read disturbance (VRD). Our extensive experiments using 160 DDR4 chips and 4 HBM2 chips from three major manufacturers yield three key observations. First, it is very unlikely that relatively few RDT measurements can accurately identify the RDT of a DRAM row. The minimum RDT of a DRAM row appears after tens of thousands of measurements (e.g., up to 94,467), and the minimum RDT of a DRAM row is $3.5\times$ smaller than the maximum RDT observed for that row. Second, the probability of accurately identifying a row’s RDT with a relatively small number of measurements reduces with increasing chip density or smaller technology node size. Third, data pattern, the amount of time an aggressor row is kept open, and temperature can affect the probability of accurately identifying a DRAM row’s RDT.

Our empirical results have implications for the security guarantees of read disturbance mitigation techniques: if the RDT of a DRAM row is not identified accurately, these techniques can easily become insecure. We discuss and evaluate using a guardband for RDT and error-correcting codes for mitigating read disturbance bitflips in the presence of RDTs that change unpredictably over time. We conclude that a $>10\%$ guardband for the minimum observed RDT combined with SECDED or Chipkill-like SSC error-correcting codes could prevent read disturbance bitflips at the cost of large read disturbance mitigation performance overheads (e.g., 45% performance loss for an RDT guardband of 50%). We hope and believe future work on efficient online profiling mechanisms and configurable read disturbance mitigation techniques could remedy the challenges imposed on today’s read disturbance mitigations by the variable read disturbance phenomenon.

1. Introduction

Read disturbance [1–6] (e.g., RowHammer and RowPress) in modern DRAM chips is a widespread phenomenon and is reliably used for breaking memory isolation [1–68], a fundamental building block for building robust systems. Repeatedly opening/activating and closing a DRAM row (i.e., aggressor

row) many times (e.g., tens of thousands of times) induces RowHammer bitflips in physically nearby rows (i.e., victim rows) [1]. Keeping the aggressor row open for a long period of time amplifies the effects of read disturbance and induces RowPress bitflips, without requiring many repeated aggressor row activations [4].

A large body of work [1, 3, 26, 32, 39, 45, 69–141] proposes various techniques to mitigate DRAM read disturbance bitflips. Many high-performance and low-overhead mitigation techniques [1, 73, 74, 76, 79, 82–84, 86, 87, 91, 97, 133–135, 137–139, 142–146], including those that are used and standardized by industry [121, 126, 138, 139, 144], prevent read disturbance bitflips by *preventively* refreshing (i.e., opening and closing) a victim row *before* a bitflip manifests in that row.

To securely prevent read disturbance bitflips at low performance and energy overhead, it is important to *accurately* identify the amount of read disturbance that a victim row can withstand before experiencing a read disturbance bitflip. This amount is typically quantified using the *hammer count* (the number of aggressor row activations) needed to induce the first read disturbance bitflip in a victim row. We call this metric the *read disturbance threshold (RDT)* of the victim row.

Prior read disturbance mitigation techniques (including those that are used and standardized by industry, e.g., PRAC [121, 126, 138, 139, 144]) assume that one can accurately (and hopefully efficiently) identify the minimum RDT across all DRAM rows in a chip.¹ In this work, we challenge this assumption and ask: *how accurately and efficiently can we measure the RDT of each row?* To this end, we rigorously characterize 160 DDR4 and 4 HBM2 DRAM chips and experimentally demonstrate that a DRAM row’s RDT *cannot* be accurately and easily (or efficiently) identified because it *changes significantly and unpredictably over time*. This is a phenomenon that has not been discussed in prior literature, and it resembles the variable retention time (VRT) phenomenon [147–153] in DRAM cells’ data retention times. We call this new phenomenon *variable read disturbance (VRD)*.

Experimental Characterization. We perform a two-step characterization study whereby we investigate the variation in RDT across 1) 100,000 repeated tests for one DRAM row in each tested DRAM chip, to draw foundational results for VRD, and 2) 1,000 repeated tests for many DRAM rows, to conduct an in-depth analysis of VRD using many data patterns, aggressor row on time (t_{AggOn}) values [4], and temperatures. Based on our novel characterization results, we provide 17 new findings and share four key takeaway lessons. Our takeaway lessons have strong implications for the security guarantees and system

¹Identifying the minimum RDT across all rows requires independently identifying the RDT of *every* DRAM row and finding the minimum value. This is because RDT *spatially* varies across rows in an unpredictable way [134].

performance, energy, and area overheads of read disturbance solutions: if the RDT of a DRAM row is *not* identified accurately, these techniques can easily become insecure.

From our 17 new findings, we hereby highlight six findings that are especially important. First, the RDT of a DRAM row changes with repeated RDT measurements (i.e., changes over time). Fig. 1 shows 100,000 successive measurements (x-axis) of the RDT (y-axis) of a victim row as an illustrative example. For the victim row shown in Fig. 1, we find the smallest RDT value after a relatively high number of 16,926 measurements. Across all tested DRAM rows from all tested DRAM chips, the smallest RDT value can appear after 94,467 measurements. 94,467 RDT measurements take approximately 9.5 seconds for a single DRAM row with a relatively small average read disturbance threshold of 1,000 (see Appendix A for RDT test time estimation methodology details). Thus, exhaustive VRD characterization of all DRAM rows in one bank of a chip easily becomes prohibitively time-intensive: approximately 29 days if the RDT of all DRAM rows (in even only a single bank of 256K rows) is measured 94,467 times.²

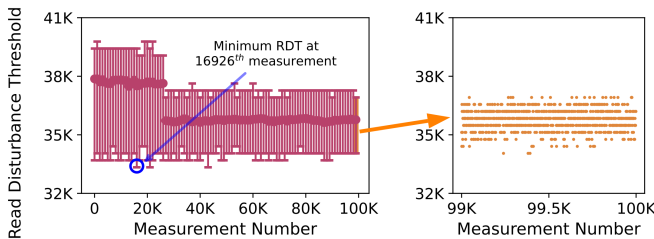


Figure 1: Read disturbance threshold (RDT) of a DRAM row over 100,000 repeated measurements (left). Each circle and error bar pair shows the distribution of RDT across 1,000 successive measurements. The circles show the mean RDT and the error bars show the range of measured RDT values. Zoomed-in view of the RDT of the row over the last 1,000 measurements (right).

Second, we analyze the distribution and predictability of the series of 100,000 RDT measurements. We find that the RDT of the tested victim rows in *all* tested DRAM chips changes significantly and *unpredictably* over time. Therefore, even *many* RDT measurements (e.g., as many as 16,926 for the DRAM row in Fig. 1) are *not* enough to absolutely guarantee that the lowest RDT is found.

Third, we find that a very large fraction (97.1%) of all tested DRAM rows exhibit VRD across *all* combinations of test parameters (temperature, t_{AggOn} , and data pattern). The remaining 2.9% of the tested rows exhibit VRD for at least one combination of test parameters. We highlight the worst-case temporal variation observed across all DRAM rows: the maximum observed RDT for a DRAM row is $3.5\times$ higher than the minimum observed RDT for that row across 1,000 RDT measurements.

Fourth, relatively few RDT measurements do *not* yield the minimum RDT expected to be found by many RDT measurements. For example, for a significant fraction (22.4%) of all tested DRAM rows, *only* one measurement across 1,000 measurements (per row) yields the minimum RDT. The maximum RDT value for such a DRAM row whose RDT is very difficult to accurately identify can be as high as $1.9\times$ the minimum RDT value observed for that row across 1,000 measurements.

²Unfortunately, due to the unpredictable nature of RDT, one would *not* know when to stop testing. Therefore, the worst-case testing time can be much longer than what we showcase here (and in the rest of the paper).

Fifth, we find that the VRD phenomenon gets worse in higher-density DRAM chips or DRAM chips manufactured using more advanced technology nodes (as indicated by the die revision). For example, with *only* one RDT measurement, we expect to find an RDT value that is 6% higher (on average across all tested DRAM rows) than the minimum observed RDT value across 1,000 measurements for the least advanced tested DDR4 chips from one manufacturer. In contrast, for the most advanced tested DDR4 chips from the same manufacturer, with *only* one RDT measurement, we expect to find an RDT value that is 8% higher than the minimum observed RDT value across 1,000 measurements.

Sixth, VRD can change with data pattern, aggressor row on time, and temperature. Therefore, producing a comprehensive VRD profile of a DRAM row requires testing each row many times for each of many different data patterns, aggressor row on time values, and temperatures.

Implications for System Security and Robustness. VRD threatens the security and robustness of existing and future read disturbance mitigation techniques. The security and robustness guarantees provided by prior read disturbance mitigation techniques rely on accurately identified RDT values across all DRAM rows in a computing system. Our results show that accurately identifying the minimum RDT across all DRAM rows, even with thousands of RDT measurements for each row, is challenging because the RDT of a row changes unpredictably over time and exhaustively testing all DRAM rows many times to uncover all possible bitflips in the presence of VRD is prohibitively time-intensive. Therefore, an approach to handling VRD will likely require tolerating some read disturbance bitflips in the presence of VRD. We evaluate the effectiveness and performance overheads of using guardbands (e.g., by configuring read disturbance mitigation techniques with an RDT value that is smaller than the minimum observed RDT) and error-correcting codes (ECC) at mitigating VRD-induced bitflips (§6). Our results suggest that a $>10\%$ guardband and single-error-correcting double-error-detecting (SECDED [154]) or Chipkill-like (e.g., single symbol correction [155–157]) ECC could prevent VRD-induced bitflips at the cost of relatively large performance overheads caused by read disturbance mitigation techniques (e.g., 45% overhead for a state-of-the-art probabilistic read disturbance mitigation technique assuming an RDT guardband of 50% and 5.9% overhead assuming a guardband of 10%).³ We call for future work on online RDT profiling and runtime configurable read disturbance mitigation techniques to remedy the challenges imposed by VRD on read disturbance mitigation techniques.

Our work makes the following contributions:

- We demonstrate that the read disturbance threshold (RDT) of a DRAM row *cannot* be reliably identified because it changes significantly and unpredictably over time. We call this phenomenon *variable read disturbance (VRD)*. We show the prevalence of VRD in modern DRAM chips.
- We present the first detailed experimental characterization of the temporal variation in DRAM read disturbance (Row-

³Our evaluation of the effectiveness and performance overheads of guardbands and error-correcting codes is based on a limited number of RDT measurements and a limited set of DRAM chips, types, and technology nodes (see §6.5). We *cannot* guarantee that using a large guardband for RDT together with ECC would prevent all read disturbance bitflips in presence of VRD.

Hammer and RowPress) in state-of-the-art DDR4 and HBM2 DRAM chips.

- We examine VRD’s major properties. One or few RDT measurements do *not* yield an RDT value that is identical or very close to the minimum RDT value observed for the same DRAM row across 1,000 measurements. This property of VRD worsens with increasing chip density and more advanced technology nodes.
- We demonstrate that VRD can change with data pattern, aggressor row on time, and temperature.
- We discuss VRD’s implications for the security and robustness of existing and future read disturbance mitigation techniques. We propose and analyze using guardbands together with ECC to reduce the impact of VRD.
- Our takeaway lessons call for future work on efficient online RDT profiling, configurable read disturbance mitigation techniques, other innovative solutions to mitigate VRD-induced bitflips, and understanding the underlying device-level causes of VRD.

2. Background and Motivation

This section provides a concise overview of 1) DRAM organization, 2) DRAM operation, 3) DRAM read disturbance, and 4) our motivation in this work.

2.1. DRAM Organization

Fig. 2 shows the organization of a DRAM-based memory system. A *memory channel* connects the processor (CPU) to a *DRAM module*, where a module consists of multiple *DRAM ranks*. A DRAM rank is formed by a set of *DRAM chips* that are operated in lockstep. Each DRAM chip has multiple *DRAM banks*. DRAM *cells* in a DRAM bank are laid out in a two-dimensional structure of rows and columns. A DRAM cell stores one bit of data in the form of electrical charge in a capacitor, which can be accessed through an access transistor. A wire called *wordline* drives the gate of all DRAM cells’ access transistors in a DRAM row. A wire called *bitline* connects all DRAM cells in a DRAM column to a common differential sense amplifier. Therefore, when a wordline is asserted, each DRAM cell in the DRAM row is connected to its corresponding sense amplifier. The set of sense amplifiers is called *the row buffer*, where the data of an activated DRAM row is buffered to serve a column access operation.

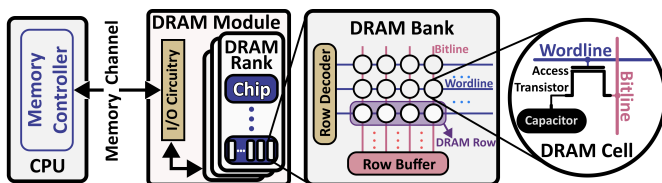


Figure 2: DRAM module, rank, chip, and bank organization

2.2. DRAM Operation

The memory controller serves memory access requests by issuing DRAM commands, e.g., row activation (*ACT*), bank precharge (*PRE*), data read (*RD*), data write (*WR*), and refresh (*REF*) while respecting certain timing parameters to guarantee correct operation [138, 158–163]. The memory controller issues an *ACT* command alongside the bank address and row address corresponding to the memory request’s address to activate a DRAM row. During the row activation process, a DRAM cell

loses its charge, and thus, its initial charge needs to be restored (via a process called *charge restoration*). The latency from the start of a row activation until the completion of the DRAM cell’s charge restoration is called the *charge restoration latency* (t_{RAS}). To access another row in an already activated DRAM bank, the memory controller must issue a *PRE* command to close the opened row and prepare the bank for a new activation.

A DRAM cell is inherently leaky and thus loses its stored electrical charge over time. To maintain data integrity, a DRAM cell is periodically refreshed with a time interval called the *refresh window* (t_{REFW}), which is typically 64 ms (e.g., [161, 162, 164]) or 32 ms (e.g., [138, 158, 159]) at normal operating temperature (i.e., up to 85 °C) and half of it for the extended temperature range (i.e., above 85 °C up to 95 °C). To refresh all cells in a timely manner, the memory controller periodically issues a refresh (*REF*) command with a time interval called the *refresh interval* (t_{REFI}), which is typically 7.8 μ s (e.g., [161, 162, 164]) or 3.9 μ s (e.g., [138, 158, 159]) at normal operating temperature. When a rank-/bank-level refresh command is issued, the DRAM chip internally refreshes several DRAM rows, during which the whole rank/bank is busy.

2.3. DRAM Read Disturbance

Read disturbance is the phenomenon in which reading data from a memory or storage device causes physical disturbance (e.g., voltage deviation, electron injection, electron trapping) on another piece of data that is *not* accessed but physically located near the accessed data. Two prime examples of read disturbance in modern DRAM chips are RowHammer [1] and RowPress [4], where repeatedly accessing (hammering) or keeping active (pressing) a DRAM row induces bitflips in physically nearby DRAM rows. In RowHammer and RowPress terminology, the row that is hammered or pressed is called the *aggressor* row, and the row that experiences bitflips the *victim* row. For read disturbance bitflips to occur, 1) the aggressor row needs to be activated more than a certain threshold value, which we call the read disturbance threshold (defined in §1), and/or 2) aggressor row on time (t_{AggOn}) [4] needs to be large enough [4, 165–167]. To avoid read disturbance bitflips, systems take preventive actions, e.g., they refresh victim rows [1, 73, 74, 76, 79, 82–84, 86, 87, 91, 97, 133–135, 137–139, 142–146], selectively throttle accesses to aggressor rows [72, 85], or physically isolate potential aggressor and victim rows [88, 89, 98, 118, 120, 168]. These solutions aim to perform preventive actions before the cumulative effect of an aggressor row’s *activation count* and *on time* causes read disturbance bitflips.

2.4. Motivation

Read disturbance has significant implications for system robustness (i.e., reliability, security, safety, and availability) because it is a widespread issue and can be exploited to break memory isolation [1–68]. Therefore, it is important to identify and understand read disturbance mechanisms in DRAM. Unfortunately, despite the existing research efforts expended towards understanding read disturbance [1, 3, 5, 6, 36, 39, 49, 52, 165–167, 169–187], scientific literature lacks a detailed understanding of a key question that is critical for robustly identifying and mitigating the read disturbance vulnerability of a system: does the read disturbance threshold of a DRAM row change over time? If so, how reliably and efficiently can it be measured? Our goal in this paper is to close this gap. We aim to empirically analyze

how reliably and efficiently the RDT of a victim DRAM row can be measured in modern DRAM chips.

3. Experimental Infrastructure

We describe our DRAM testing infrastructure and the real DDR4 and HBM2 DRAM chips tested.

DRAM Testing Setup. We build our testing setup on DRAM Bender [186, 188], an open-source FPGA-based DRAM testing infrastructure (which builds on SoftMC [189, 190]). This setup consists of four main components 1) a host machine that generates the test program and collects experimental results, 2) an FPGA development board (AMD Alveo U200 [191] for DDR4 and Alveo U50 [192] and Bittware XUPVH [193] for HBM2 DRAM chips), programmed with DRAM Bender to execute test programs and analyze experimental data, 3) a thermocouple-based temperature sensor and a pair of heater pads pressed against the DRAM chips that heat up the DRAM chips to a desired temperature, and 4) a PID temperature controller (MaxWell FT200 [194]) that keeps the temperature at the desired level with a precision of $\pm 0.5^\circ\text{C}$.

Tested DRAM Chips. Table 1 shows the 160 DDR4 DRAM chips (in 21 modules) and 4 HBM2 DRAM chips that we test from all three major DRAM manufacturers. To investigate whether VRD is affected by different DRAM technologies, designs, and manufacturing processes, we test various DRAM chips with different densities, die revisions, chip organizations, and DRAM standards.

Table 1: Tested DDR4 Modules and HBM2 Chips

Mfr.	DDR4 Module	# of Chips	Density Die Rev.	Chip Org.	Date (ww-yy)
Mfr. H (SK Hynix)	H0	8	8Gb - J	x8	N/A
	H1	8	16Gb - C	x8	36-21
	H2	8	8Gb - A	x8	43-18
	H3, H4	8	8Gb - D	x8	38-19
	H5, H6	8	8Gb - D	x8	24-20
Mfr. M (Micron)	M0	4	16Gb - E	x16	46-20
	M1	8	16Gb - F	x8	37-22
	M2	8	16Gb - F	x8	37-22
	M3, M4	8	8Gb - R	x8	12-24
	M5	8	8Gb - R	x8	10-24
	M6	8	16Gb - F	x8	12-24
Mfr. S (Samsung)	S0	8	8Gb - C	x8	N/A
	S1	8	8Gb - B	x8	53-20
	S2	8	8Gb - D	x8	10-21
	S3	8	16Gb - A	x8	20-23
	S4	4	4Gb - C	x16	19-19
	S5, S6	8	16Gb - B	x16	15-23
Mfr. S (Samsung)	HBM2 Chip Chip0 - Chip3	4	N/A	N/A	N/A

3.1. Testing Methodology

Disabling Sources of Interference. We identify three factors that can interfere with our results: 1) data retention failures [149, 195], 2) on-die read disturbance defense mechanisms (e.g., TRR [39, 45, 196]), and 3) error correction codes (ECC) [163, 197, 198]. We carefully reuse the state-of-the-art read disturbance characterization methodology used in prior works to eliminate the interference factors [4, 5, 45, 134, 165–167, 185]. First, we make sure that our experiments finish strictly within a refresh window, in which the DRAM manufacturers guarantee that *no* retention bitflips occur [161, 163]. Second, we disable periodic refresh as doing so disables all known

on-die read disturbance defense mechanisms [45, 165–167]. Third, we verify that the tested DDR4 chips do *not* have on-die ECC [197, 198], we do *not* use rank-level ECC in our testing setup, and we disable the tested HBM2 chips’ ECC by setting the corresponding HBM2 mode register bit to zero [163].

RowHammer and RowPress Access Pattern. We use the double-sided RowHammer and RowPress access pattern [1, 4, 16, 165, 166], which alternately activates two aggressor rows physically adjacent to a victim row. We record the bitflips observed in the row between two aggressor rows.

Logical-to-Physical Row Mapping. DRAM manufacturers use mapping schemes to translate logical (memory-controller-visible) addresses to physical row addresses [1, 11, 29, 40, 85, 149, 166, 197, 199–206]. To identify aggressor rows that are physically adjacent to a victim row, we reverse-engineer the row mapping scheme following the methodology described in prior work [166].

RowHammer and RowPress Test Parameters. We perform multiple different tests with varying test parameters. We explain the common parameters in this section and elaborate on the detailed parameters of each test in §4 and §5. We configure tests by tuning four parameters: 1) *Hammer count*: We define the *hammer count* of a double-sided read disturbance access pattern as the number of activations *each* aggressor row receives. Therefore, in a double-sided RowHammer or a RowPress test with a hammer count of 10, we activate each of the two aggressor rows 10 times, resulting in a total of 20 row activations. 2) *Aggressor row on time (t_{AggOn})*: The time each aggressor row stays open after each activation during a RowHammer or a RowPress test. 3) *Data pattern*: We use the four data patterns (Table 2) that are widely used in memory reliability testing [207] and by prior work on DRAM characterization (e.g., [1, 4, 5, 134, 165, 166]). 4) *Temperature*: We use a temperature controller setup for all DDR4 modules and one HBM2 DRAM chip (Chip 0) and set the target temperature to 50°C , 65°C , or 80°C , depending on the type of experiment performed. Even though we do not have the same temperature controller setups for HBM2 DRAM chips, Chip1-3, we perform these experiments in a temperature-controlled room. We monitor the in-HBM2-chip temperature sensor using the IEEE 1500 test port [163] and verify that Chip1, Chip2, and Chip3’s temperatures are stable across all our tests, such that maximum temperature deviation is 2.0°C over 24 hours of continuous testing.

Table 2: Data patterns used in our experiments

Row Addresses	Rowstripe0	Rowstripe1	Checked0	Checked1
Victim (V)	0x00	0xFF	0x55	0xAA
Aggressors ($V \pm 1$)	0xFF	0x00	0xAA	0x55
$V \pm [2:8]$	0x00	0xFF	0x55	0xAA

Read Disturbance Threshold. We quantify the read disturbance vulnerability of a DRAM row using the *read disturbance threshold (RDT)* metric, i.e., the *hammer count needed to induce the first read disturbance bitflip* in the victim row.

4. Foundational Results

We investigate the variation in read disturbance threshold (RDT) across repeated tests. We measure RDT in all tested DDR4 and HBM2 DRAM chips 100,000 times. Our experimental results demonstrate that the RDT of a DRAM row changes *unpredictably* across repeated RDT measurements.

DRAM Testing Algorithm. Alg. 1 shows our test routine in two steps. First, `find_victim` (line 1 in Alg. 1) identifies a DRAM row that is relatively more vulnerable to read disturbance to be the subject of our extensive tests. To do so, we choose a row that exhibits RDT values below 40,000 for the minimum t_{AggOn} (e.g., 35 ns) on average across ten successive measurements using the Checkered0 data pattern.⁴ The first step yields a *guessed RDT value* (RDT_{guess}) for the tested DRAM row, as the row’s mean RDT value across 10 RDT measurements. Second, `test_loop` (line 12 in Alg. 1) repeatedly measures the RDT of the identified victim row. We do so by testing the DRAM row for read disturbance failures using hammer counts ranging from $RDT_{guess}/2$ to $RDT_{guess} * 3$ with increments of $RDT_{guess}/100$.⁵ This experiment yields a series of 100,000 RDT measurements for each tested row. To draw foundational results for VRD, we perform 100,000 RDT measurements using one DRAM row in each tested DDR4 module and HBM2 chip. §5 shows more extensive results using many DRAM rows, data patterns, t_{AggOn} values, and temperatures.

Algorithm 1: Test for profiling the temporal variation of read disturbance in DRAM

```

// RA_victim: Victim row address
// HC: Hammer count, activations per aggressor row
// VDP: Victim row's data pattern
// LRA: The largest row address in the tested chip
// t_AggOn: Aggressor row on time
1 Function find_victim(VDP, t_AggOn):
2   foreach RA_victim in range(0, LRA) do
3     // Guess RDT of the victim row
4     // by repeatedly measuring it for 10 times
5     // the guess is the mean RDT across all 10 measurements
6     RDT_guess = guess_rdt(RA_victim, VDP, t_AggOn)
7     if RDT_guess < 40,000 then
8       | return RDT_guess, RA_victim
9     end
10  end
11
12 Function test_loop():
13  RDT_guess, RA_victim = find_victim(VDP, t_AggOn)
14  RDT_min = RDT_guess/2
15  RDT_max = RDT_guess * 3
16  RDT_step = RDT_guess/100
17  foreach measurement_number in range(0, 100,000) do
18    foreach RDT in range(RDT_min, RDT_max, RDT_step) do
19      initialize_rows(RA_victim, VDP)
20      hammer_doublesided(RA_victim, RDT, t_AggOn)
21      bit_flip = compare_data(RA_victim, VDP)
22      if bit_flip then
23        | write RDT to storage
24        | break
25      end
26    end
27  end

```

Results. Fig. 3 shows the distribution of all values in the series of 100,000 measured RDT values (y-axis) for each tested DDR4

⁴To maintain a reasonable experiment time, we select one combination of test parameters (e.g., we test one relatively more read-disturbance-vulnerable victim DRAM row) used in our RDT testing experiments in this section. §5 shows more extensive results with a wider range of test parameters (e.g., more DRAM rows, data patterns, t_{AggOn} values, and temperatures).

⁵We empirically determine the range and the granularity of the tested hammer count values such that our experiments take reasonable time and cover a wide range of RDTs that the DRAM row may exhibit.

module and HBM2 chip (x-axis) in a box-and-whiskers plot.⁶ Each point in a box is the outcome of one RDT measurement.

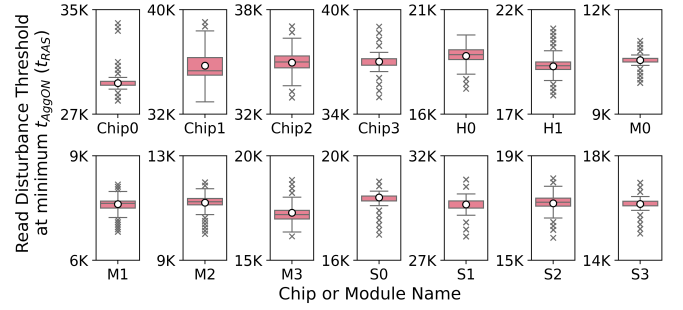


Figure 3: RDT distribution of a single victim row in each tested module and chip

Finding 1. A DRAM row’s RDT changes over time.

We observe that the RDTs of all tested DRAM rows significantly change across repeated measurements. For example, for the victim row in Chip0, the largest measured RDT is $1.21 \times$ the smallest measured RDT, across 100,000 measurements.

To better depict how RDT varies over time, Fig. 4 shows the histogram of the measured RDT values of one selected victim row in each tested module and chip.

Finding 2. The RDT of a row has multiple states.

We make three key observations from Fig. 4. First, the RDT of a row takes various different values across 100,000 measurements, i.e., the RDT of a row has multiple states. For example, we measure 21 unique RDT values across 100,000 measurements on DDR4 module M1. Second, for the majority of tested DRAM rows (13 out of 14), the measured RDT values are accumulated around a mean RDT value. Third, we observe that the RDT values in HBM Chip1 follow a bimodal distribution, unlike other tested chips.

We analyze how long a DRAM row retains the same RDT value across subsequent measurements. Fig. 5 shows a histogram of the number of consecutive measurements across which a DRAM row exhibits the same RDT value, aggregated across all 14 tested rows. The x-axis shows the number of consecutive RDT measurements yielding the same RDT value. For example, the bar at $x = 1$ shows the number of two consecutive RDT measurements yielding *different* RDT values, and the bar at $x = 2$ shows the number of two consecutive RDT measurements yielding *the same* RDT value.

Finding 3. The RDT of a row frequently changes over time.

We make two key observations. First, two consecutive RDT measurements likely yield different RDT values, i.e., the RDT of a row frequently changes over time. Across all tested rows, 79.0% of RDT state changes happen after every measurement. Second, as the number of consecutive measurements increases (as we go right on the x-axis), the likelihood of those measurements yielding the same value decreases. A row retains the same RDT value for 14 consecutive RDT measurements very rarely (i.e., in *only one* instance).

⁶The box is lower-bounded by the first quartile (i.e., the median of the first half of the ordered set of data points) and upper-bounded by the third quartile (i.e., the median of the second half of the ordered set of data points). The interquartile range (IQR) is the distance between the first and third quartiles (i.e., box size). Whiskers show the minimum and maximum values. The circles show the mean of all data points.

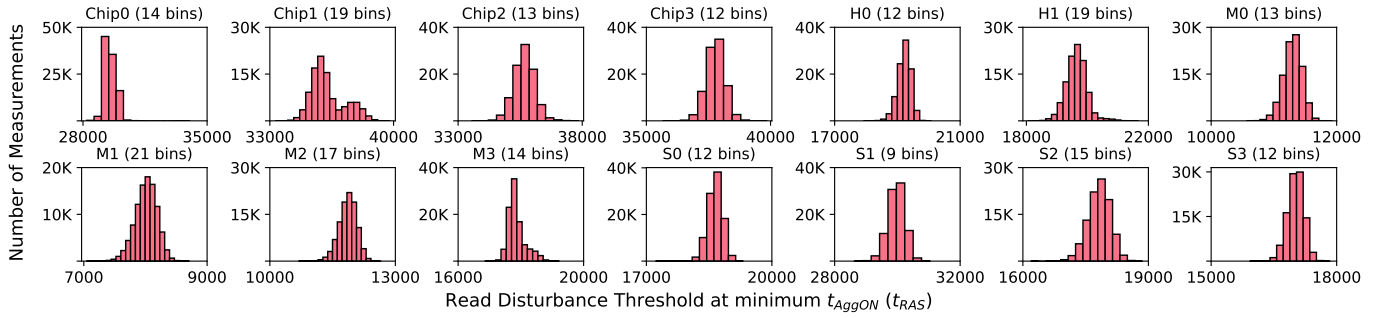


Figure 4: Histogram of RDT values for a single victim row in each tested module and chip. We indicate the number of unique measured RDT values as the number of bins. Each bin in a subplot has an equal width. Bin size is computed as the range of RDT values (max - min) on the x-axis divided by the number of unique measured RDT values.

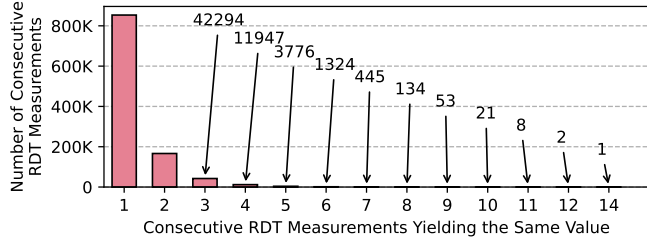


Figure 5: Histogram of the number of measurements across which a row's RDT exhibits the same value

4.1. Predictability of RDT's Temporal Variation

We have established that there is temporal variation in the RDT of a DRAM row. We draw a preliminary analysis of the *predictability* of the temporal variation in RDT.

Finding 4. *A row's RDT changes unpredictably over time.*

Our analysis suggests that individual RDT measurements are likely unpredictable, that is, given the outcome of past RDT measurements for a victim row, the outcome of the next measurement likely *cannot* be predicted.⁷ We perform a two-step analysis to understand the predictability of the temporal variation in RDT. First, we carefully interpret the histograms of the RDT values in Fig. 4. Second, we compute the autocorrelation function of the values to detect repeating patterns.

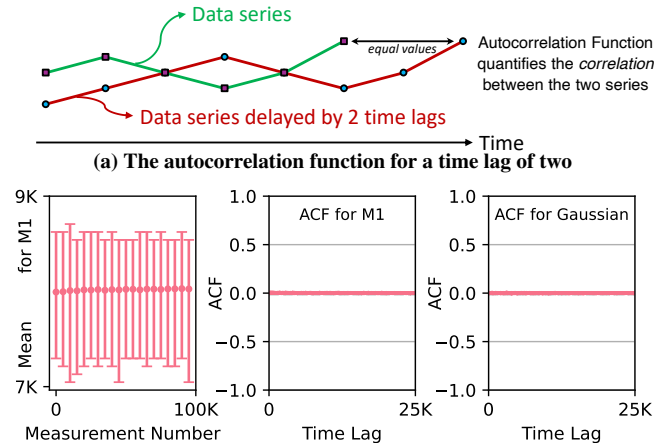
Histogram Interpretation. Many of the RDT histograms resemble prominent random (discrete) probability distributions. For example, from a visual inspection, the histograms for M1, H1, and Chip2 strongly suggest that the RDT measurements follow the probability density function of a normal distribution. To quantify how well the frequency of the RDT measurements resembles a normal distribution derived from the mean and the standard deviation of all RDT measurements, we perform the Chi-square goodness-of-fit test [208]. For each tested chip, the Chi-square goodness-of-fit test tests the null hypothesis (H_0) that our observations follow the derived normal distribution. H_0 holds if the Chi-square test outputs a p-value greater than a chosen level of significance denoted as α . We find the minimum p-value across all tested chips to be 0.18. Thus, at $\alpha = 0.05$, we *cannot* reject the null hypothesis that our data follows the derived normal distribution. We conclude that an RDT measurement likely samples a normally distributed random variable.

Analyzing Repeating Patterns. Fig. 1 shows the distributions of the series of RDT measurements of one tested victim row (in

⁷The frequency of RDT values collected over many RDT measurements, however, are predictable based on the probability distributions (histograms) shown in Fig. 4.

Chip1). From a visual inspection, we *cannot* identify any obvious repeating patterns in RDT measurements. The measured RDT values from other victim rows on other chips also yield distributions that do *not* harbor repeating patterns.

To strengthen our observation that a series of RDT measurements does *not* harbor a repeating pattern, we methodically analyze the RDT measurements using the autocorrelation function (ACF) [209]. ACF quantifies the correlation between the series of RDT measurements with a delayed (by a time lag) copy of the same series, pictorially depicted in Fig. 6a. Fig. 6b shows the series of RDT measurements (circles show the mean and error bars show the minimum and maximum RDT values across 1,000 successive measurements for a single row), the ACF of this series, and the ACF of a series of 100,000 normally distributed random numbers.



(b) The series of RDT measurements for one row in DRAM module M1 (left), its ACF (middle), and the ACF of a series of 100,000 normally distributed random numbers (right)

Figure 6: The autocorrelation function (ACF) (top) and ACF analysis of RDT measurements from module M1 (bottom)

We observe that the ACF of the series of RDT measurements is *not* significantly different than the ACF of a normally distributed random variable. We make similar observations for other series of RDT measurements from other DRAM modules and chips. We conclude that a series of 100,000 successive RDT measurements likely does *not* harbor repeating patterns.

Takeaway 1. RDT changes randomly and unpredictably. As such, reliably and accurately identifying the RDT of a DRAM row is challenging.

4.2. Hypothetical Explanation for VRD

We provide a hypothetical explanation that could explain why and how RDT temporally varies.⁸ Electron migration and injection into the victim cell is a major error mechanism that leads to DRAM read disturbance bitflips [172, 175, 176, 187, 210, 211]. Prior works [175, 176, 187, 210, 211] show that the electron migration and injection mechanism is heavily assisted by charge traps in the shared active region of the aggressor and victim cell and its Si/SiO₂ interface. We hypothesize that the temporal variation in RDT can be attributed to the randomly changing occupied/unoccupied states of these traps [212, 213]. This hypothetical explanation is similar to the explanation of the variable retention time (VRT) phenomenon [147–153].⁹ More device-level studies are needed to build confidence for our hypothesis that the observed temporal variation is based on unpredictable physical phenomena. We leave a more detailed investigation of device-level mechanisms that cause the temporal variation in RDT (including its relationship with DRAM variable retention time) for future work.

5. In-Depth Analysis of VRD

In this section, we further enhance our analysis of the *variable read disturbance* (VRD) phenomenon by investigating parameters that have been shown to impact RDT [4, 167]. Concretely, first, we analyze how VRD changes across DRAM rows, die densities, and die revisions. Second, we evaluate VRD with different 1) data patterns, 2) t_{AggOn} , and 3) temperature ranges. Our results show that 1) all tested DRAM rows exhibit VRD, 2) VRD is worse in higher-density DRAM chips and or chips with more advanced technology nodes, 3) data pattern affects VRD differently across tested DRAM chips, and 4) VRD can change with t_{AggOn} and temperature.

Test Parameters. We test 150 DRAM rows in each tested DDR4 chip. To select the 150 DRAM rows, we measure the RDT of each DRAM row in the first, middle, and last 1024 DRAM rows in a DRAM bank in each tested DDR4 chip 10 times. From each of the first, middle, and last 1024 DRAM rows, we select 50 DRAM rows with the smallest mean RDT values across 10 measurements. We test 150 DRAM rows from three HBM2 channels (50 randomly selected DRAM rows from each channel) in four HBM2 chips. We use the data patterns listed in Table 2. We use three t_{AggOn} values: 1) the minimum t_{RAS} timing parameter as defined in the DRAM standard, 2) t_{REFI} , the average interval between two successive periodic refresh commands, 3) $9 \times t_{REFI}$, the maximum interval between two subsequent periodic refresh commands (i.e., the maximum time a row can remain open according to the DDR4 [161] and

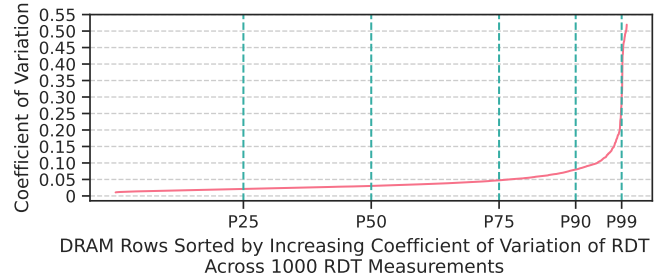
⁸We are not aware of any device-level study of temporal variations in read disturbance vulnerability, so we *cannot* definitively confirm this hypothesis. That said, we are unable to identify any independent variables within our control that allow reliably predicting the minimum RDT despite extensive testing.

⁹The observed temporal variation in RDT (i.e., VRD) may differ from the observed temporal variation in DRAM cell retention times (i.e., VRT). Unfortunately, there is *not* enough available scientific information to confidently explain such differences between VRD and VRT. We do *not* know enough about the underlying causes of VRD and we believe that VRD should be studied independently of VRT. We hope and expect that future device-level studies (inspired by this work) will develop a better understanding of the inner workings of VRD as device-level studies (e.g., [210, 211]) did for RowPress *after* the RowPress paper [4] demonstrated the empirical basis for the RowPress phenomenon. We believe such studies could provide insight into the (hypothesized) similarities and differences between VRT and VRD.

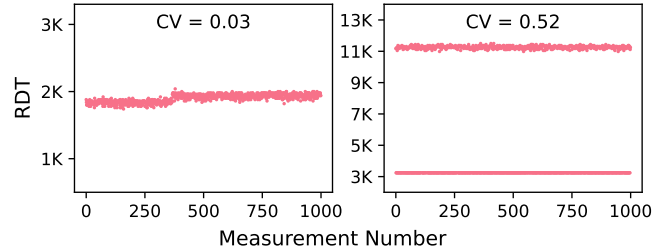
HBM2 standards [163]). We test DRAM chips at 50 °C, 65 °C, and 80 °C using our temperature controller setup (§3.1).

5.1. VRD Across DRAM Rows

Fig. 7a shows an S-curve of the coefficient of variation (CV)¹⁰ (y-axis) across all tested DRAM rows sorted in increasing CV (x-axis). We plot the maximum observed CV for each tested DRAM row in every DRAM chip across all combinations of test parameters (data pattern, t_{AggOn} , and temperature). A higher CV indicates a larger variance around the mean RDT value across 1,000 RDT measurements. Fig. 7b shows the RDT measurement results (y-axis) across 1,000 measurements (x-axis) for the two rows that mark the P50 (50th percentile, the middle point in the figure) and P100 (100th percentile, the right-most point, not marked in Fig. 7a) points in Fig. 7a on the left- and right-hand side, respectively.



(a) Variation in a row’s read disturbance threshold values across 1,000 measurements



(b) Measured read disturbance threshold values of two rows across 1,000 successive measurements. P50 row with CV = 0.03 (left) and the P100 row with the greatest CV = 0.52 (right).

Figure 7: Temporal variation of RDT across DRAM rows

Finding 5. All tested rows exhibit temporal RDT variation.

All tested DRAM rows have non-zero CV in at least one combination of tested data patterns, t_{AggOn} values, and temperatures. The maximum CV across all tested rows is 0.52. We observe that 50% of rows (to the right of P50 on the x-axis) have greater than 0.03 CV. We observe that the read disturbance threshold varies from 1740 to 2040 (by a factor of 1.2 \times) and from 3242 to 11498 (by a factor of 3.5 \times) for the DRAM row on the left subplot and the DRAM row on the right subplot, respectively.

Finding 6. A large fraction (97.1%) of tested DRAM rows exhibit temporal variation across all test parameters.

For 97.1% of the tested DRAM rows, under *all* combinations of test parameters (data pattern, t_{AggOn} , and temperature), the measured RDT values vary across 1,000 measurements (not shown in Fig. 7). In contrast, the RDT values do *not* change with 1,000 repeated measurements for 2.9% of the tested DRAM rows under at least one combination of test parameters. However, at least one test parameter combination yields multiple

¹⁰Coefficient of variation is the standard deviation of all 1,000 RDT measurements normalized to the mean across all 1,000 RDT measurements.

RDT values across 1,000 measurements for such DRAM rows. **Probability of Identifying the Minimum RDT.** Based on our analyses in §4, measuring the RDT of a DRAM row is similar to sampling from a probability distribution. Thus, we analyze 1) the probability of identifying the minimum RDT value of a DRAM row across 1,000 measurements with $N < 1,000$ measurements, which we call the *probability of finding the minimum RDT* with N measurements and 2) the expected value of the minimum RDT across $N < 1,000$ measurements normalized to the minimum RDT across 1,000 measurements, which we call the *expected normalized value of the minimum RDT* across N measurements. To do so, we run Monte Carlo simulations for 10,000 iterations. In each iteration, we uniformly randomly select N RDT measurements from the series of 1,000 measurements for each tested DRAM row. We repeat the simulations for $N = 1, 3, 5, 10, 50,$ and 500 , and for each combination of test parameters, to demonstrate how the probability of finding the minimum RDT and the expected normalized value of the minimum RDT changes with the number of RDT measurements.

Fig. 8 shows 1) the distribution of the probability of finding the minimum RDT across tested rows (top) and 2) the distribution of the expected normalized value of the minimum RDT across tested rows (middle) for number of measurements (N) in the range $[1, 500]$ on the x-axis, and 3) the expected normalized value of the minimum RDT over the probability of finding the minimum RDT (bottom) for $N = 1, 50,$ and 500 (we plot only three values to ease readability).¹¹ Each box in the top and middle figures shows the distribution across all tested DRAM rows and all combinations of test parameters. We consider VRD to be worse for DRAM rows that exhibit a *smaller* probability of finding the minimum RDT and a *greater* expected normalized value of the minimum RDT. For example, a $y = 1.5$ for the expected normalized value of the minimum RDT means that, with N measurements (depicted on the x-axis in the top and middle subplots in Fig. 8), we expect to find an RDT that is 50% higher than the minimum value we would find if we performed 1,000 RDT measurements. The DRAM rows that are closer to the top left corner in the bottom plot indicate the DRAM rows that exhibit the worst VRD behavior.

Finding 7. *It is very unlikely to find the minimum RDT of a DRAM row with $N = 1$ RDT measurement.*

One RDT measurement for the median DRAM row (P50) has a 0.2% probability of yielding the minimum RDT across 1,000 measurements (Fig. 8 top). For 22.4% of the tested DRAM rows, the probability of finding the minimum RDT among 1,000 measurements using only a single measurement is $\leq 0.1\%$.

Finding 8. *The value of the minimum RDT across 1,000 measurements is significantly smaller than the one expected to be found with $N = 1$ RDT measurement.*

To make matters worse, a DRAM row whose RDT is unlikely to be identified with a single measurement can also exhibit a very large variation in its RDT (top left corner of Fig. 8 bottom). The expected normalized value of the minimum RDT for those DRAM rows with a *low* ($\leq 0.1\%$) probability of finding the minimum RDT can be as high as $1.9\times$ the minimum RDT across 1,000 measurements ($1.1\times$ on average across all rows with $\leq 0.1\%$ probability of finding the minimum RDT). In contrast,

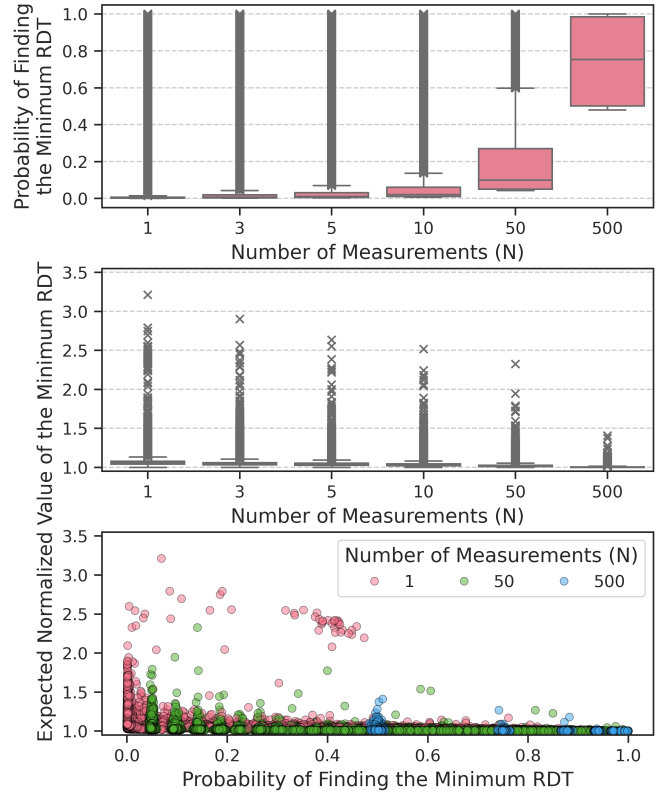


Figure 8: Probability of finding the minimum RDT with $N < 1,000$ measurements (top); the expected value of the minimum RDT found with $N < 1,000$ measurements normalized to the minimum RDT across 1,000 measurements (middle); the expected normalized value of the minimum RDT over the probability of finding the minimum RDT (bottom)

only 5.4% of the tested DRAM rows exhibit a high probability of finding the minimum RDT (i.e., $\geq 99.9\%$) using a single measurement. For those DRAM rows with a high probability of finding the minimum RDT using a single measurement, the expected normalized value of the minimum RDT is relatively small: at most $1.001\times$.

Finding 9. *The probability of finding the minimum RDT of a DRAM row increases with the number of RDT measurements.*

With $N = 1, 3, 5, 10, 50,$ and 500 measurements, the median DRAM row (P50) has 0.2%, 0.7%, 1.1%, 2.1%, 10.0%, and 75.3% probability of finding the minimum RDT across 1,000 measurements, respectively. We observe that even at a relatively high number of $N = 500$ RDT measurements, a DRAM row may exhibit a relatively low probability of finding the minimum RDT of approximately 50.0% (bottom tail of the rightmost box in Fig. 8 top). For such a DRAM row, *only 1* out of 1,000 measurements yields the minimum RDT value.

We conclude that all tested DRAM rows exhibit temporal variation in RDT, and the minimum RDT (across 1,000 measurements) of the majority of DRAM rows *cannot* be found with a high probability (e.g., $>90\%$) using 500 measurements. A DRAM row’s expected RDT value obtained using a single measurement can be $1.9\times$ the minimum RDT observed for that row across 1,000 measurements, and this minimum RDT value may appear only *once* across the series of 1,000 measurements.

¹¹Fig. 25 shows a larger version of the bottom plot in Fig. 8 with $N = 1, 3, 5, 10, 50,$ and 500 .

Takeaway 2. Relatively few (e.g., $N < 500$) RDT measurements are unlikely to identify the minimum RDT value of a DRAM row. Estimations for the minimum RDT of a DRAM row can become more accurate with repeated RDT measurements but RDT *cannot* be found easily (even after $N = 500$ measurements) with a high probability.

5.2. Effect of Die Density and Die Revision

To understand if and how DRAM technology scaling affects VRD, we investigate how the distribution of observed RDT values changes with the die density and the die revision of the tested DRAM chips. Fig. 9 shows the distribution (across 150 tested rows per module) of the expected normalized value of the minimum RDT for varying number of measurements (N) in the range $[1, 500]$ on the x-axis. Each subplot shows the distribution for a different DRAM chip manufacturer in a box-and-whiskers plot.⁶ Different boxes show the distribution for one combination of the die density and die revision¹² of tested DRAM chips. We refer to the range of expected normalized value of the minimum RDT distribution (as depicted by each box in the figure) as the *VRD profile* of a DRAM chip. A higher box in the figure depicts a "worse" VRD profile: if we perform only N measurements, we will likely be farther off from the minimum RDT we would find if we had performed 1,000 measurements.

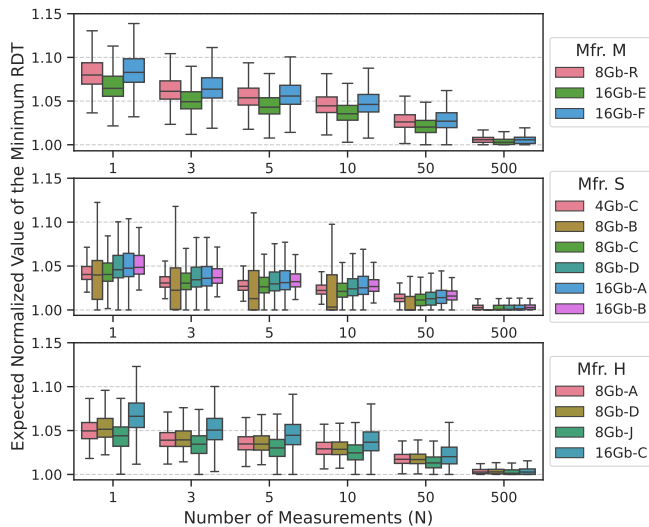


Figure 9: Expected normalized value of the minimum RDT after N measurements across DDR4 chip die densities and die revisions

Finding 10. VRD profile varies across tested DRAM chips.

Across tested Mfr. M, Mfr. S, and Mfr. H chips, the median DRAM row (and the worst-case DRAM row, not shown in the figure) has a $1.08\times$ ($1.84\times$), $1.05\times$ ($3.21\times$), and $1.05\times$ ($1.70\times$) expected normalized value of the minimum RDT for $N = 1$ RDT measurement, respectively. This means that with one measurement only, we expect to find an RDT that is $3.21\times$ the minimum value we would find if we had performed 1,000 RDT measurements for the *worst-case row* from all tested chips.

Finding 11. VRD profile worsens with increasing die density and with advanced DRAM technology.

¹²For a given manufacturer and die density, the later in the alphabetical order the die revision code is, the more likely the chip has a more advanced technology node.

In general, the higher the density of the DRAM chip or the more advanced the technology node (as indicated by the die revision)¹², the worse the VRD profile. For example, the expected normalized value of the minimum RDT using $N = 1$ measurement for the median DRAM row (and for the worst-case row, not shown in the figure) increases to $1.08\times$ ($1.78\times$) from $1.06\times$ ($1.45\times$) for Mfr. M's chips as the chip density increases and the technology node advances. We observe similar trends for all manufacturers and tested values of N .

We conclude that different DRAM chips experience different VRD profiles. The VRD profile of a chip gets worse in higher-density chips or chips with more advanced technology nodes.

5.3. Effect of Data Pattern

We analyze how the VRD profiles of the tested chips change with data patterns used to initialize aggressor and victim DRAM rows. Fig. 10 shows the distribution (across tested rows) of the expected normalized value of the minimum RDT for varying number of measurements (N) listed on the x-axis in a box-and-whiskers plot.⁶ Each subplot is for a different DRAM chip manufacturer (and the bottom subplot is for the tested HBM2 chips), and each box shows the distribution of the expected values for a different data pattern.

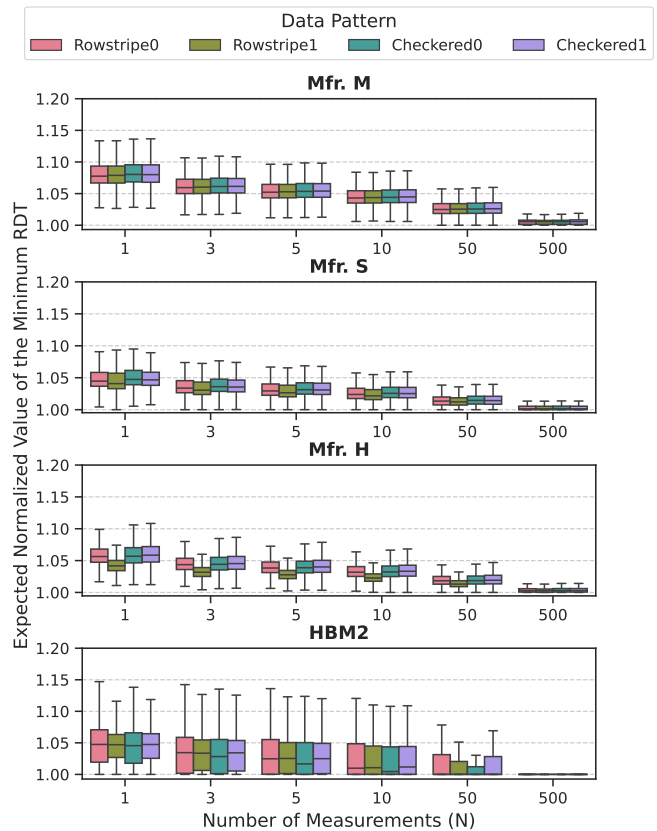


Figure 10: Expected normalized value of the minimum RDT after N measurements across four tested data patterns

Finding 12. VRD profile of a DRAM chip changes with data pattern.

For example, the median DRAM row (and the worst-case row, not shown in the figure) in an Mfr. H DRAM chip has an expected normalized value of the minimum RDT using $N = 1$ measurement ranging from $1.04\times$ ($1.57\times$) to $1.06\times$ ($1.70\times$) for

different data patterns. We observe that the data pattern affects the VRD profile in all DDR4 chips from all manufacturers (and in HBM2 chips) for all tested numbers of measurement values.

Finding 13. *No single data pattern causes the worst VRD profile across all tested DRAM chips.*

The data pattern that yields the largest expected normalized value of the minimum RDT with $N = 1$ RDT measurement is Checkered0, Rowstripe1, Rowstripe0, and Checkered1 for the median row across all tested DRAM chips from Mfr. M, Mfr. S, Mfr. S HBM2, and Mfr. H, respectively.

Takeaway 3. How the lowest RDT varies over time depends on the data pattern.

5.4. Effect of Aggressor Row On Time

We investigate the sensitivity of VRD to the amount of time an aggressor row is kept open (t_{AggOn}). Fig. 11 shows the distribution (across tested rows) of the expected normalized value of the minimum RDT for varying number of measurements (N) listed on the x-axis in a box-and-whiskers plot.⁶ Each subplot is for a different DRAM chip manufacturer (and the bottom subplot is for the tested HBM2 chips), and each box shows the distribution of the expected values for a t_{AggOn} .

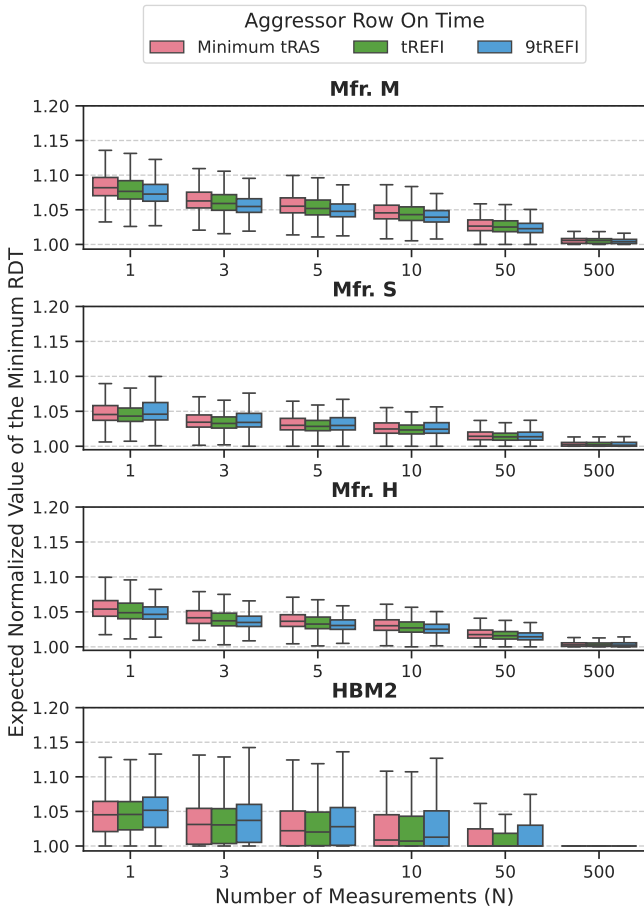


Figure 11: Expected normalized value of the minimum RDT after N measurements across three tested t_{AggOn} values

Finding 14. *VRD profile changes with t_{AggOn} .*

For example, the median DRAM row (and the worst-case DRAM row, not shown in the figure) across all rows in all tested

Mfr. H chips has $1.054 \times (1.602 \times)$, $1.049 \times (1.597 \times)$, and $1.046 \times (1.467 \times)$ expected normalized value of the minimum RDT using $N = 1$ RDT measurement for t_{AggOn} values of minimum t_{RAS} (approximately 35 ns), t_{REFI} (7.8 μ s in DDR4 [161]), and $9 \times t_{REFI}$ (70.2 μ s in DDR4 [161]), respectively.

Finding 15. *VRD profile can become better or worse as t_{AggOn} increases.*

For example, the tested Mfr. M and Mfr. H DRAM chips display a decreasing expected normalized value of the minimum RDT as t_{AggOn} increases. For the tested Mfr. S chips, the median expected normalized value of the minimum RDT across all tested rows is lower at $t_{AggOn} = t_{REFI}$ and higher at $t_{AggOn} = \text{minimum } t_{RAS}$ and $9 \times t_{REFI}$.

5.5. Effect of Temperature

Fig. 12 shows the distribution of the expected normalized value of the minimum RDT with *one RDT measurement* for six selected example DRAM chips, two from Mfr. M (top), two from Mfr. S (middle), and two from Mfr. H (bottom) using the Rowstripe1 data pattern and for $t_{AggOn} = \text{minimum } t_{RAS}$ in a box-and-whiskers plot.⁶ Different boxes show the distribution of the expected values for different temperatures.

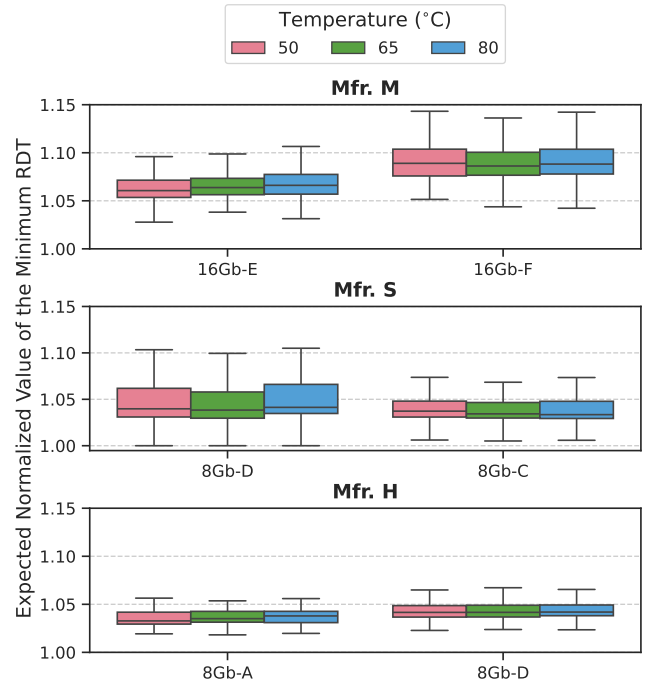


Figure 12: Expected normalized value of the minimum RDT with one RDT measurement for the Rowstripe1 data pattern at $t_{AggOn} = \text{minimum } t_{RAS}$

Finding 16. *VRD profile of a DRAM chip changes with temperature.*

As temperature increases from 50 °C to 80 °C, the expected value of the minimum RDT for the median DRAM row (and for the worst-case row, not shown in the figure) in an Mfr. M 16Gb-E die chip increases from $1.06 \times (1.22 \times)$ to $1.07 \times (1.29 \times)$. Our finding that VRD profile changes with temperature is consistent across all tested t_{AggOn} values and data patterns.

We conclude that aggressor row on time and temperature both affect VRD. We do *not* identify any prominent correlation between VRD, t_{AggOn} , and temperature from our empirical data.

Takeaway 4. Temperature and t_{AggOn} affect VRD. The VRD profile at one temperature level and one t_{AggOn} value likely would *not* resemble the VRD profile across all operating temperatures and t_{AggOn} values.

5.6. Effect of True- and Anti-Cell Layout

We study VRD’s sensitivity to DRAM cell data *encoding conventions* [1, 149, 197, 198, 214, 215] (i.e., *true-cell* and *anti-cell*) used in the victim row. Each DRAM cell in a DRAM chip may store data using two encoding conventions: 1) a true-cell encodes a “logic-1” as a fully-charged capacitor, or 2) an anti-cell encodes a “logic-1” as a fully-discharged capacitor. We experimentally measure the layout of true- and anti-cells throughout 50 randomly selected victim DRAM rows in module M0 using the methodology described in prior works [1, 214, 215]. Figure 13 shows the distribution of the coefficient of variation (y-axis) across 1,000 RDT measurements for each of the tested 20 DRAM rows with anti-cells (left box) and 30 DRAM rows with true-cells (right box). The figure shows the distribution for all tested data patterns (left subplot), temperature levels (middle subplot), and aggressor row on times (right subplot) in a box-and-whiskers plot.⁶

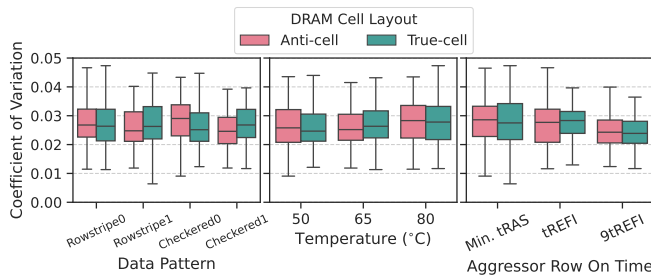


Figure 13: Coefficient of variation across 1,000 RDT measurements on 20 DRAM rows with anti-cells (left box) and 30 DRAM rows with true-cells (right box) for different data patterns (left subplot), temperature levels (middle subplot), and aggressor row on times (right subplot)

Finding 17. The presence of true- and anti-cells in the victim row does not significantly affect the RDT distribution in one tested module (M0).

6. Implications of VRD for Read Disturbance Mitigation Techniques

The key takeaways we draw from our empirical study have important implications for the security guarantees of read disturbance mitigation techniques, proposed by both academia and industry (e.g., [1, 79, 83, 85, 87, 88, 91, 93, 98, 111, 115, 118, 126, 133–137, 139–142, 144]) and some already standardized for immediate system integration (e.g., PRAC [121, 126, 138, 139, 144]). At a high level, the security guarantees provided by any of these mitigation techniques rely on an accurately identified *minimum read disturbance threshold (RDT) across all DRAM rows in a computing system*. Our results show that accurately identifying the minimum RDT across all DRAM rows, even with thousands of RDT measurements, is challenging because the RDT of a row changes over time in an unpredictable way (Takeaway 1).

We evaluate and discuss the effectiveness of combining a guardband for RDT (e.g., by reducing the minimum observed RDT by an arbitrary factor when configuring mitigation techniques) with error-correcting codes (ECC) at mitigating VRD-

induced bitflips (i.e., read disturbance bitflips in the presence of VRD). We show that using a $>10\%$ guardband for the minimum observed RDT along with single-error-correcting double-error-detecting (SEDED [154]) ECC or Chipkill-like ECC (e.g., single symbol error correction [155–157]) could prevent VRD-induced bitflips at the cost of potentially higher performance overheads incurred by read disturbance mitigation techniques that are configured with smaller read disturbance threshold values (due to applying a guardband). We believe future work on online RDT profiling and runtime configurable read disturbance mitigation techniques could remedy the challenges imposed by VRD on read disturbance mitigation techniques.

6.1. Importance of Accurately Identifying RDT

There are two reasons that make accurate identification of RDT important for read disturbance mitigation techniques: 1) security and 2) system performance, energy, and area overheads. First, the RDT value used to configure a mitigation technique *cannot* be larger than the one experienced (at any time) by any victim DRAM row in a DRAM chip. Otherwise, the mitigation technique’s security guarantees are compromised. For example, PRAC [121, 126, 138, 139, 144], if configured with an RDT value that is larger than the smallest RDT of a DRAM row, would eventually fail to prevent a read disturbance bitflip if this DRAM row is hammered or pressed. Second, the configured RDT value should *not* be significantly smaller than the one experienced by any victim DRAM row, as smaller RDT values lead to higher system performance, energy, and area or storage overheads [85, 87, 133, 134, 139, 144, 165].

6.2. Challenges of Accurately Identifying RDT

Measuring the RDT of a DRAM row hundreds of times is *not* sufficient for drawing a comprehensive profile for the RDT of the DRAM row (Takeaways 1 and 2). The difference between the minimum and maximum RDT of a DRAM row can be more than $3.5\times$ after 1,000 measurements (see Finding 5) and may not be bounded.¹³ While repeated RDT measurements can lead to a better minimum RDT estimate for a DRAM row (Takeaway 2), VRD is affected by data pattern, t_{AggOn} , and temperature (Takeaways 3 and 4), which makes comprehensive RDT profiling time-intensive because state-of-the-art integrated circuit test times are measured in seconds to minutes [216, 217], while as few as *only* two RDT measurements (for all DRAM rows in one bank) can require hours of testing. For example, measuring the RDT of each DRAM row in a bank *only once* with a hammer count of 8,000, using four data patterns, at $t_{AggOn} = \text{minimum } t_{RAS}$, and at three temperature levels takes approximately 39 minutes for a *single* DRAM bank of 256K rows (see Appendix A for read disturbance threshold test time estimation methodology details and test time demonstrations).

6.3. Overheads of Using a Guardband for RDT

To determine the RDT of a DRAM row, a system designer or a DRAM manufacturer might measure RDT a few times (to minimize testing time) and apply a safety margin (i.e., a guardband) to the minimum observed RDT value. To understand the performance overheads of using a guardband for RDT, we evaluate four state-of-the-art mitigation techniques (Graphene [83], PRAC [138], PARA [1], and MINT [218]) in a DDR5-based

¹³See discussion on limitations of our experimental methodology in §6.5.

computing system simulated using a cycle-level memory system simulator, Ramulator 2.0 [219, 220] (based on Ramulator [221, 222]). Fig. 14 shows system performance with the four mitigation techniques normalized to the baseline system that does *not* implement read disturbance mitigation using 15 four-core highly memory intensive workload mixes.¹⁴ The x-axis shows eight different read disturbance threshold values; the first four representing a near-future RDT of 1024 with 0%, 10%, 25%, and 50% safety margins and the last four representing a future, very-low RDT of 128 with 0%, 10%, 25%, and 50% safety margins. We make two key observations.¹⁵

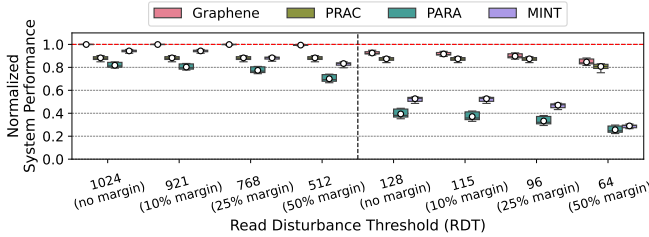


Figure 14: Four-core highly memory intensive workload performance normalized to the baseline system without read disturbance mitigation for two different read disturbance threshold values, each with four different levels of safety margin (guardband) added

First, a small but potentially unsafe 10% safety margin for RDT does *not* significantly increase mitigation performance overheads at RDT=1024 and =128. For example, performance with Graphene, PRAC, PARA, and MINT using a 10% safety margin for RDT=128 reduces by 1.0%, 0.0%, 5.9%, and 0.0%, respectively, compared to no margin.¹⁶ Second, a relatively aggressive but much safer safety margin of 50% substantially increases performance overheads incurred by mitigation techniques. For example, performance with Graphene, PRAC, PARA, and MINT using a 50% safety margin at RDT=128 reduces by 8.5%, 7.6%, 35.0%, and 45.0%, respectively, compared to no margin. We conclude that the performance overheads incurred with four state-of-the-art read disturbance mitigation techniques substantially increase with a larger guardband for RDT. Based on our analysis, we do *not* recommend relying solely on guardbands to address the temporal variation in RDT.

¹⁴We use 57 single-core workloads from SPEC CPU2006 [223], SPEC CPU2017 [224], TPC [225], MediaBench [226], and YCSB [227] to construct 15 four-core workload mixes. We consider a workload to be highly memory intensive if it has an LLC MPKI (last level cache misses per kilo instruction) that is ≥ 20 . Graphene (memory-controller-based) [83] and PRAC (in-DRAM) [138] have storage overhead and track the activation count of an aggressor row using hardware counters and preventively refresh the aggressor row’s neighbors before the activation count reaches the configured read disturbance threshold. PARA (memory-controller-based) [1] and MINT (in-DRAM) [218] do *not* have storage overhead and determine the target row of a DRAM activate command as an aggressor row based on a probability that is determined based on the configured RDT and preventively refresh the aggressor row’s neighbors.

¹⁵Prior works characterize real DRAM chips and observe that safety margins for DRAM command timing parameters can be $>40\%$ [228] and safety margins for data retention times can be even larger [149].

¹⁶PRAC and MINT’s performance overheads do *not* increase as RDT reduces from 128 to 115 because the number and the frequency of PRAC and MINT’s preventive actions (e.g., DRAM-initiated back-offs [138] and RFM commands [138]) do *not* change as RDT reduces from 128 to 115.

6.4. Effectiveness of Guardbands & ECC Against VRD

To quantitatively assess the effectiveness of using guardbands for RDT, we analyze the probability of finding the minimum observed RDT of a DRAM row across 1,000 measurements within 10%, 20%, 30%, 40%, and 50% of the minimum observed RDT of that DRAM row using $N < 1,000$ measurements via the testing methodology described in §5. Fig. 15 shows the mean (circles) and minimum (bars) probability of finding the minimum RDT (across all tested rows and combinations of test parameters) within a safety margin indicated by the color of the circle or the bar as the number of measurements (N) increases from 1 to 500 (x-axis). For example, for $N = 50$ measurements, the red (leftmost) circle indicates the *average* probability of 50 RDT measurements yielding a value that is within 10% of the minimum RDT value observed across 1,000 measurements, across all rows and combinations of test parameters (which is $y = 0.991$). The red (leftmost) bar under the red circle indicates the *minimum* probability of 50 RDT measurements yielding a value that is within 10% of the minimum RDT value observed across 1,000 measurements, across all tested rows and combinations of test parameters (which is $y = 0.045$).

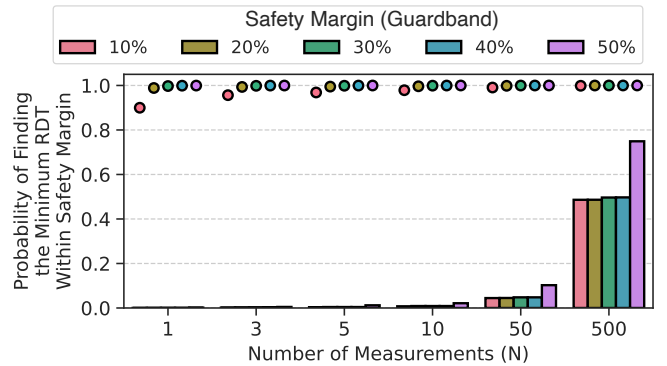


Figure 15: Probability of finding the minimum RDT with $N < 1,000$ measurements using a safety margin. Circles show the mean and bars show the minimum probability across all tested rows.

We make two major observations. First, even with $N = 50$ (500) measurements, the average probability of finding the minimum RDT is 99.07% (99.86%) with a small safety margin (10%), and the minimum probability is even lower, i.e., 4.46% (48.62%). Second, with $N = 500$ measurements, the minimum probability of finding the minimum RDT is *only* 74.91% with a *large* safety margin (50%), i.e., even a large guardband does *not* guarantee that the minimum RDT is always identified. We conclude that using safety margins (guardbands) alone is likely *not* effective at mitigating VRD-induced read disturbance bitflips.

We conduct an experiment to understand the effectiveness of combining a guardband for RDT with ECC at preventing VRD-induced bitflips. We conclude that a $>10\%$ guardband for the observed minimum RDT and single-error-correcting double-error-detecting (SECCED) or Chipkill-like (SSC) ECC could potentially (but likely not safely) prevent VRD-induced read disturbance bitflips. In the experiment, we use Checkered0 and Checkered1 data patterns (see Table 2), and set $t_{AggOn} = \text{minimum } t_{RAS}$. We keep the temperature of the tested DRAM chips at 50 °C. We use the DDR4 DRAM modules used in §5 and test 50 DRAM rows in each module. We 1) measure the RDT of

each tested DRAM row 5 times (to maintain a reasonable testing time) to find the minimum RDT for the tested DRAM row and 2) repeatedly test the DRAM row for read disturbance failures using RDT safety margins of 50%, 40%, 30%, 20%, and 10% for 10,000 times. For example, if the first step of the experiment yields an RDT of 500 for a DRAM row, we repeatedly test the DRAM row 10,000 times for each of the hammer count values of 250, 300, 350, 400, and 450. Fig. 16 shows the histogram for the number of unique bitflips in a DRAM row (when we use a safety margin of 10%) across 10,000 RDT measurements.



Figure 16: Number of unique bitflips in a DRAM row when we use a safety margin of 10%. The histogram shows the distribution of the number of unique bitflips across all tested rows.

We make two key observations. First, there are up to 5 unique DRAM cells that experience read disturbance bitflips in a DRAM row across 10,000 measurements at a safety margin of 10%. The bitflips manifest in up to 4 different DRAM chips on the DRAM module and there is at most one bitflip in a single-error correcting and double-error detecting (SECDED) [154] or a Chipkill-like ECC (e.g., single symbol error correction [155–157]) codeword. Therefore, the observed bitflips (in this *very limited* set of experiments) likely lead to error patterns that are correctable by SECDED [154] and Chipkill-like ECC [155–157]. However, the presence of VRD-induced bitflips in different DRAM chips suggests that VRD could yield *multiple* read disturbance bitflips in one ECC codeword, which could result in uncorrectable or undetectable errors and lead to silent data corruptions (SDCs), albeit infrequently (Table 3 quantifies the probability of such VRD-induced errors, as we explain soon, and shows high likelihood of SDCs even with Chipkill-like ECC). With more RDT measurements, we may see more bitflips and higher silent data corruption rates. Second, for safety margins larger than 10%, we do *not* observe more than one bitflip in the tested DRAM rows across 10,000 measurements (not shown in Fig. 16).

We quantify the probability of uncorrectable errors (i.e., SDCs) assuming the worst error rate we observed empirically so far that results in 5 bitflips in a 64 Kibit DRAM row ($7.6e-5$ bit error rate) for a 10% safety margin. Table 3 shows the probability of uncorrectable, undetectable, and uncorrectable but detectable errors for single-error-correcting (SEC [154]) code and single-error-correcting double-error-detecting (SECDED [154]) code using a 72-bit codeword, and single-symbol-correcting (Chipkill-like, SSC [156]) code using a 144-bit codeword with 18 symbols in a codeword.

From Table 3, we observe that VRD-induced bitflips could cause uncorrectable errors with a relatively low probability based on the empirically observed error rate using a safety margin of 10%. Higher safety margins ($>10\%$) and ECC could prevent VRD-induced read disturbance errors given the limited measurement dataset presented in this work. However, a

Table 3: Probability of uncorrectable, undetectable, and detectable uncorrectable errors at the worst error rate we observed empirically so far ($7.6e-5$) using an RDT safety margin of 10% for SEC, SECDED, and Chipkill-like SSC codes. N/A indicates the result category does not exist for the shown ECC type.

Type of error	SEC	SECDED	Chipkill-like (SSC)
Uncorrectable	1.48e-05	1.48e-05	5.66e-05
Undetectable	1.48e-05	2.64e-08	5.66e-05
Detectable uncorrectable	N/A	1.48e-05	N/A

more detailed analysis of error rates is needed to make a definitive conclusion and doing so requires a dedicated large-scale characterization study that performs many more measurements (e.g., millions or billions of RDT measurements over time) as opposed to 1K or 10K. We leave such a study to future work.

6.5. Discussion and Future Work

The major contribution of this work is the observation of the VRD phenomenon and its first experimental characterization, demonstrating that a DRAM row’s RDT *cannot* be accurately and easily (or efficiently) identified because it changes significantly and unpredictably over time. Our results have implications for the security guarantees of read disturbance mitigation techniques: if the RDT of a DRAM row is *not* identified accurately, these techniques become insecure.

The implications of VRD for read disturbance mitigation techniques resemble the implications of variable retention time (VRT) for DRAM retention-aware intelligent refresh mechanisms (e.g., [149, 151, 153, 195, 204, 229–234]). If previously undiscovered read disturbance bitflips are a permanent possibility, then any approach to handling VRD will require tolerating some read disturbance bitflips in the presence of VRD, possibly via the use of error-correcting codes or message authentication codes (MACs) [96, 235], and a guardband.

While our experimental results indicate that using a $>10\%$ guardband for the observed minimum RDT and ECC could potentially (but likely not safely) prevent VRD-induced read disturbance bitflips, our results are limited: we 1) perform only 1K or 10K measurements (instead of millions or billions), 2) test a limited number, type, and technology node of DRAM chips (160 DDR4 and four HBM2 chips; Table 1), and 3) test a limited set of environmental conditions and process corners (e.g., voltage and temperature variations). Therefore, we *cannot* guarantee that using a (large) guardband for RDT along with ECC would prevent all VRD-induced bitflips. Moreover, the effects of VRD might continue to worsen with increasing DRAM die density and with advanced DRAM technology (Finding 11) such that VRD-induced bitflips become more costly to mitigate using a guardband and ECC.

We believe there are at least three promising directions for future work: 1) gather more data, more comprehensively, by performing more RDT measurements, testing more DRAM chips, and testing with a wider variety of environmental conditions and process corners (e.g., voltage, and temperature variations), 2) develop online RDT profiling mechanisms to efficiently profile DRAM chips while the chips are in use in order to mitigate the long RDT profiling times implied by our results, and 3) develop new read disturbance mitigation techniques that can dynamically configure their read disturbance threshold by cooperating with online profiling mechanisms.

7. Related Work

To our knowledge, this is the first work to experimentally demonstrate and comprehensively examine *temporal variation* in read disturbance behavior in modern DRAM chips, and provide potential solutions to mitigate its effects. In this section, we discuss other relevant prior work.

Experimental Read Disturbance Characterization. Prior works extensively characterize the RowHammer and RowPress vulnerabilities in real DRAM chips [1, 4, 5, 134, 165–167, 182, 185, 236–238]. These works demonstrate (using real DDR3, DDR4, LPDDR4, and HBM2 DRAM chips) how a DRAM chip’s read disturbance vulnerability varies with 1) DRAM refresh rate [1, 39, 45], 2) the physical distance between aggressor and victim rows [1, 165, 236], 3) DRAM generation and technology node [1, 45, 165, 166], 4) temperature [166, 170], 5) the time the aggressor row stays active [4, 5, 166, 170, 185, 237, 238], 6) physical location of the victim DRAM cell [5, 134, 166, 185], 7) wordline voltage [167], and 8) supply voltage [182]. None of these works analyze *temporal variation* in read disturbance.

System-Level RowHammer Tests. Several works [40, 239–241] develop tools or RowHammer tests that aim to identify read disturbance bitflips in DRAM chips in a computing system. These tools and tests could prove useful in developing future efficient online RDT profiling techniques.

Retention Failure Profiling. Prior works [149, 151, 153, 195, 204] advocate and propose methods to efficiently profile DRAM retention failures that are subject to the variable retention time (VRT) phenomenon. These works could inspire or aid the development of online RDT profiling techniques.

8. Conclusion

We present the results of the first detailed characterization study of the temporal variation of the read disturbance (RowHammer and RowPress) vulnerability in modern DDR4 and HBM2 DRAM chips. We demonstrate that the read disturbance threshold (RDT) of a DRAM row *cannot* be reliably identified even with hundreds or thousands of measurements because the RDT of a row changes significantly and unpredictably over time. Our study leads to 17 findings and four takeaway lessons which have important implications for future read disturbance mitigation techniques: if the RDT of a DRAM row is not identified accurately, these techniques can easily become insecure. We study potential solutions to mitigate the effects of VRD and find that 1) using a small guardband for the observed minimum RDT (when configuring read disturbance mitigation techniques) along with error-correcting codes is likely unsafe and 2) using a large guardband along with error-correcting codes can lead to high performance overheads. We hope and expect that our findings will lead to a deeper understanding of and new solutions to the read disturbance vulnerabilities in modern DRAM-based computing systems.

Acknowledgments

We thank the anonymous reviewers of HPCA 2025 and our shepherd for feedback. We thank the SAFARI Research Group members for constructive feedback and the stimulating intellectual environment. We acknowledge the generous gift funding provided by our industrial partners (especially Google, Huawei, Intel, Microsoft), which has been instrumental in enabling the research we have been conducting on read disturbance in DRAM

in particular and memory systems in general [242]. This work was in part supported by the Google Security and Privacy Research Award and the Microsoft Swiss Joint Research Center.

References

- [1] Y. Kim, R. Daly, J. Kim, C. Fallin, J. H. Lee, D. Lee, C. Wilkerson, K. Lai, and O. Mutlu, “Flipping Bits in Memory Without Accessing Them: An Experimental Study of DRAM Disturbance Errors,” in *ISCA*, 2014.
- [2] O. Mutlu and J. Kim, “RowHammer: A Retrospective,” *IEEE TCAD Special Issue on Top Picks in Hardware and Embedded Security*, 2019.
- [3] O. Mutlu, A. Olgun, and A. G. Yaglikci, “Fundamentally Understanding and Solving RowHammer,” in *ASP-DAC*, 2023.
- [4] H. Luo, A. Olgun, A. G. Yaglikci, Y. C. Tuğrul, S. Rhyner, M. B. Cavlak, J. Lindeger, M. Sadrosadati, and O. Mutlu, “RowPress: Amplifying Read Disturbance in Modern DRAM Chips,” in *ISCA*, 2023.
- [5] A. Olgun, M. Osseiran, A. G. Yaglikci, Y. C. Tuğrul, H. Luo, S. Rhyner, B. Salami, J. G. Luna, and O. Mutlu, “Read Disturbance in High Bandwidth Memory: A Detailed Experimental Study on HBM2 DRAM Chips,” in *DSN*, 2024.
- [6] O. Mutlu, “The RowHammer Problem and Other Issues We May Face as Memory Becomes Denser,” in *DATe*, 2017.
- [7] A. P. Fournaris, L. Pocero Fraile, and O. Koufopavlou, “Exploiting Hardware Vulnerabilities to Attack Embedded System Devices: A Survey of Potent Microarchitectural Attacks,” *Electronics*, 2017.
- [8] D. Poddebniak, J. Somorovsky, S. Schinzel, M. Lochter, and P. Rösler, “Attacking Deterministic Signature Schemes using Fault Attacks,” in *EuroS&P*, 2018.
- [9] A. Tatar, R. K. Konoth, E. Athanasopoulos, C. Giuffrida, H. Bos, and K. Razavi, “Throhammer: Rowhammer Attacks Over the Network and Defenses,” in *USENIX ATC*, 2018.
- [10] S. Carre, M. Desjardins, A. Facon, and S. Guillel, “OpenSSL Bellcore’s Protection Helps Fault Attack,” in *DSD*, 2018.
- [11] A. Barengi, L. Breveglieri, N. Izzo, and G. Pelosi, “Software-only Reverse Engineering of Physical DRAM Mappings for Rowhammer Attacks,” in *IVSW*, 2018.
- [12] Z. Zhang, Z. Zhan, D. Balasubramanian, X. Koutsoukos, and G. Karsai, “Triggering Rowhammer Hardware Faults on ARM: A Revisit,” in *ASHES*, 2018.
- [13] S. Bhattacharya and D. Mukhopadhyay, “Advanced Fault Attacks in Software: Exploiting the Rowhammer Bug,” in *Fault Tolerant Architectures for Cryptography and Hardware Security*, 2018.
- [14] M. Seaborn and T. Dullien, “Exploiting the DRAM Rowhammer Bug to Gain Kernel Privileges,” <http://googleprojectzero.blogspot.com.tr/2015/03/exploiting-dram-rowhammer-bug-to-gain.html>, 2015.
- [15] SAFARI Research Group, “RowHammer — GitHub Repository,” <https://github.com/CMU-SAFARI/rowhammer>, 2014.
- [16] M. Seaborn and T. Dullien, “Exploiting the DRAM Rowhammer Bug to Gain Kernel Privileges,” *Black Hat*, 2015.
- [17] V. van der Veen, Y. Fratantonio, M. Lindorfer, D. Gruss, C. Maurice, G. Vigna, H. Bos, K. Razavi, and C. Giuffrida, “Drammer: Deterministic Rowhammer Attacks on Mobile Platforms,” in *CCS*, 2016.
- [18] D. Gruss, C. Maurice, and S. Mangard, “Rowhammer.js: A Remote Software-Induced Fault Attack in Javascript,” in *DIMVA*, 2016.
- [19] K. Razavi, B. Gras, E. Bosman, B. Preneel, C. Giuffrida, and H. Bos, “Flip Feng Shui: Hammering a Needle in the Software Stack,” in *USENIX Security*, 2016.
- [20] P. Pessl, D. Gruss, C. Maurice, M. Schwarz, and S. Mangard, “DRAMA: Exploiting DRAM Addressing for Cross-CPU Attacks,” in *USENIX Security*, 2016.
- [21] Y. Xiao, X. Zhang, Y. Zhang, and R. Teodorescu, “One Bit Flips, One Cloud Flops: Cross-VM Row Hammer Attacks and Privilege Escalation,” in *USENIX Security*, 2016.
- [22] E. Bosman, K. Razavi, H. Bos, and C. Giuffrida, “Dedup Est Machina: Memory Deduplication as An Advanced Exploitation Vector,” in *S&P*, 2016.
- [23] S. Bhattacharya and D. Mukhopadhyay, “Curious Case of RowHammer: Flipping Secret Exponent Bits using Timing Analysis,” in *CHES*, 2016.
- [24] W. Burleson, O. Mutlu, and M. Tiwari, “Invited: Who is the Major Threat to Tomorrow’s Security? You, the Hardware Designer,” in *DAC*, 2016.
- [25] R. Qiao *et al.*, “A New Approach for RowHammer Attacks,” in *HOST*, 2016.
- [26] F. Brasser, L. Davi, D. Gens, C. Liebchen, and A.-R. Sadeghi, “Can’t Touch This: Software-Only Mitigation Against Rowhammer Attacks Targeting Kernel Memory,” in *USENIX Security*, 2017.
- [27] Y. Jang, J. Lee, S. Lee, and T. Kim, “SGX-Bomb: Locking Down the Processor via Rowhammer Attack,” in *SysTEX*, 2017.
- [28] M. T. Aga, Z. B. Aweke, and T. Austin, “When Good Protections Go Bad: Exploiting Anti-DOS Measures to Accelerate Rowhammer Attacks,” in *HOST*, 2017.
- [29] A. Tatar, C. Giuffrida, H. Bos, and K. Razavi, “Defeating Software Mitigations Against Rowhammer: A Surgical Precision Hammer,” in *RAID*, 2018.
- [30] D. Gruss, M. Lipp, M. Schwarz, D. Genkin, J. Juffinger, S. O’Connell, W. Schoechl, and Y. Yarom, “Another Flip in the Wall of Rowhammer Defenses,” in *S&P*, 2018.
- [31] M. Lipp, M. T. Aga, M. Schwarz, D. Gruss, C. Maurice, L. Raab, and L. Lamster, “Nethammer: Inducing Rowhammer Faults Through Network Requests,” arXiv:1805.04956, 2018.
- [32] V. van der Veen, M. Lindorfer, Y. Fratantonio, H. P. Pillai, G. Vigna, C. Kruegel, H. Bos, and K. Razavi, “GuardION: Practical Mitigation of DMA-Based Rowhammer Attacks on ARM,” in *DIMVA*, 2018.
- [33] P. Frigo, C. Giuffrida, H. Bos, and K. Razavi, “Grand Pwning Unit: Accelerating Microarchitectural Attacks with the GPU,” in *S&P*, 2018.
- [34] L. Cojocar, K. Razavi, C. Giuffrida, and H. Bos, “Exploiting Correcting Codes: On the Effectiveness of ECC Memory Against Rowhammer Attacks,” in *S&P*, 2019.
- [35] S. Ji, Y. Ko, S. Oh, and J. Kim, “Pinpoint Rowhammer: Suppressing Unwanted Bit Flips on Rowhammer Attacks,” in *ASIACCS*, 2019.
- [36] O. Mutlu, “RowHammer and Beyond,” in *COSADE*, 2019.

- [37] S. Hong, P. Frigo, Y. Kaya, C. Giuffrida, and T. Dumitras, "Terminal Brain Damage: Exposing the Graceless Degradation in Deep Neural Networks Under Hardware Fault Attacks," in *USENIX Security*, 2019.
- [38] A. Kwong, D. Genkin, D. Gruss, and Y. Yarom, "RAMBleed: Reading Bits in Memory Without Accessing Them," in *S&P*, 2020.
- [39] P. Frigo, E. Vannacci, H. Hassan, V. van der Veen, O. Mutlu, C. Giuffrida, H. Bos, and K. Razavi, "TRRespass: Exploiting the Many Sides of Target Row Refresh," in *S&P*, 2020.
- [40] L. Cojocar, J. Kim, M. Patel, L. Tsai, S. Saroiu, A. Wolman, and O. Mutlu, "Are We Susceptible to Rowhammer? An End-to-End Methodology for Cloud Providers," in *S&P*, 2020.
- [41] Z. Weissman, T. Tiemann, D. Moghimi, E. Custodio, T. Eisenbarth, and B. Sunar, "JackHammer: Efficient Rowhammer on Heterogeneous FPGA-CPU Platforms," arXiv:1912.11523, 2020.
- [42] Z. Zhang, Y. Cheng, D. Liu, S. Nepal, Z. Wang, and Y. Yarom, "PTHammer: Cross-User-Kernel-Boundary Rowhammer Through Implicit Accesses," in *MICRO*, 2020.
- [43] F. Yao, A. S. Rakin, and D. Fan, "Deephammer: Depleting the Intelligence of Deep Neural Networks Through Targeted Chain of Bit Flips," in *USENIX Security*, 2020.
- [44] F. de Ridder, P. Frigo, E. Vannacci, H. Bos, C. Giuffrida, and K. Razavi, "SMASH: Synchronized Many-Sided Rowhammer Attacks from JavaScript," in *USENIX Security*, 2021.
- [45] H. Hassan, Y. C. Tugrul, J. S. Kim, V. van der Veen, K. Razavi, and O. Mutlu, "Uncovering In-DRAM Rowhammer Protection Mechanisms: A New Methodology, Custom Rowhammer Patterns, and Implications," in *MICRO*, 2021.
- [46] P. Jattke, V. van der Veen, P. Frigo, S. Gunter, and K. Razavi, "Blacksmith: Scalable Rowhammering in the Frequency Domain," in *S&P*, 2022.
- [47] M. C. Tol, S. Islam, B. Sunar, and Z. Zhang, "Toward Realistic Backdoor Injection Attacks on DNNs using RowHammer," arXiv:2110.07683, 2022.
- [48] A. Kogler, J. Juffinger, S. Qazi, Y. Kim, M. Lipp, N. Boichat, E. Shiu, M. Nissler, and D. Gruss, "Half-Double: Hammering From the Next Row Over," in *USENIX Security*, 2022.
- [49] L. Orosa, U. Rührmair, A. G. Yaglıkci, H. Luo, A. Olgun, P. Jattke, M. Patel, J. Kim, K. Razavi, and O. Mutlu, "SpyHammer: Understanding and Exploiting RowHammer Under Fine-Grained Temperature Variations," *IEEE Access*, 2024.
- [50] Z. Zhang, W. He, Y. Cheng, W. Wang, Y. Gao, D. Liu, K. Li, S. Nepal, A. Fu, and Y. Zou, "Implicit Hammer: Cross-Privilege-Boundary Rowhammer through Implicit Accesses," *IEEE TDSC*, 2022.
- [51] L. Liu, Y. Guo, Y. Cheng, Y. Zhang, and J. Yang, "Generating Robust DNN with Resistance to Bit-Flip based Adversarial Weight Attack," *TC*, 2022.
- [52] Y. Cohen, K. S. Tharayil, A. Haenel, D. Genkin, A. D. Keromytis, Y. Oren, and Y. Yarom, "HammerScope: Observing DRAM Power Consumption Using Rowhammer," in *CCS*, 2022.
- [53] M. Zheng, Q. Lou, and L. Jiang, "TrojViT: Trojan Insertion in Vision Transformers," arXiv:2208.13049, 2022.
- [54] M. Fahr Jr, H. Kippen, A. Kwong, T. Dang, J. Lichtinger, D. Dachman-Soled, D. Genkin, A. Nelson, R. Perlner, A. Yerukhimovich *et al.*, "When Frodo Flips: End-to-End Key Recovery on FrodoKEM via Rowhammer," *CCS*, 2022.
- [55] Y. Tobah, A. Kwong, I. Kang, D. Genkin, and K. G. Shin, "SpecHammer: Combining Spectre and Rowhammer for New Speculative Attacks," in *S&P*, 2022.
- [56] A. S. Rakin, M. H. I. Chowdhury, F. Yao, and D. Fan, "DeepSteal: Advanced Model Extractions Leveraging Efficient Weight Stealing in Memories," in *S&P*, 2022.
- [57] H. Aydin and A. Serbaş, "Cyber Security in Industrial Control Systems (ICS): A Survey of RowHammer Vulnerability," *Applied Computer Science*, 2022.
- [58] K. Mus, Y. Doröz, M. C. Tol, K. Rahman, and B. Sunar, "Jolt: Recovering TLS Signing Keys via Rowhammer Faults," *Cryptology ePrint Archive*, 2022.
- [59] J. Wang, H. Xu, C. Xiao, L. Zhang, and Y. Zheng, "Research and Implementation of Rowhammer Attack Method based on Domestic NeoKylin Operating System," in *ICFTIC*, 2022.
- [60] S. Lefforge, "Reverse Engineering Post-Quantum Cryptography Schemes to Find Rowhammer Exploits," Bachelor's Thesis, University of Arkansas, 2023.
- [61] M. J. Fahr, "The Effects of Side-Channel Attacks on Post-Quantum Cryptography: Influencing FrodoKEM Key Generation Using the Rowhammer Exploit," Master's thesis, University of Arkansas, 2022.
- [62] A. Kaur, P. Srivastav, and B. Ghoshal, "Work-in-Progress: DRAM-MaUT: DRAM Address Mapping Unveiling Tool for ARM Devices," in *CASES*, 2022.
- [63] K. Cai, Z. Zhang, and F. Yao, "On the Feasibility of Training-time Trojan Attacks through Hardware-based Faults in Memory," in *HOST*, 2022.
- [64] D. Li, D. Liu, Y. Ren, Z. Wang, Y. Sun, Z. Guan, Q. Wu, and J. Liu, "Cyber-Radar: A PUF-based Detecting and Mapping Framework for Physical Devices," arXiv:2201.07597, 2022.
- [65] A. Roohi and S. Angizi, "Efficient Targeted Bit-Flip Attack Against the Local Binary Pattern Network," in *HOST*, 2022.
- [66] F. Staudigl, H. Al Indari, D. Schön, D. Sisejkovic, F. Merchant, J. M. Joseph, V. Rana, S. Menzel, and R. Leupers, "NeuroHammer: Inducing Bit-Flips in Memristive Crossbar Memories," in *DATE*, 2022.
- [67] L.-H. Yang, S.-S. Huang, T.-L. Cheng, Y.-C. Kuo, and J.-J. Kuo, "Socially-Aware Collaborative Defense System against Bit-Flip Attack in Social Internet of Things and Its Online Assignment Optimization," in *ICCCN*, 2022.
- [68] S. Islam, K. Mus, R. Singh, P. Schaumont, and B. Sunar, "Signature Correction Attack on Dilithium Signature Scheme," in *Euro S&P*, 2022.
- [69] Apple Inc., "About the Security Content of Mac EFI Security Update 2015-001," <https://support.apple.com/en-us/HT204934>, 2015.
- [70] Hewlett-Packard Enterprise, "HP Moonshot Component Pack Version 2015.05.0," <http://h17007.www1.hp.com/usa/en/enterprise/servers/products/moonshot/component-pack/index.aspx>, 2015.
- [71] Lenovo, "Row Hammer Privilege Escalation," https://support.lenovo.com/us/en/product_security/row_hammer, 2015.
- [72] Z. Greenfield and T. Levy, "Throttling Support for Row-Hammer Counters," 2016, U.S. Patent 9,251,885.
- [73] D.-H. Kim, P. J. Nair, and M. K. Qureshi, "Architectural Support for Mitigating Row Hammering in DRAM Memories," *IEEE CAL*, 2014.
- [74] K. S. Bains and J. B. Halbert, "Distributed Row Hammer Tracking," U.S. Patent: 9,299,400, 2016.
- [75] K. Bains *et al.*, "Method, Apparatus and System for Providing a Memory Refresh," U.S. Patent: 9,030,903, 2015.
- [76] Z. B. Aweke, S. F. Yitbarek, R. Qiao, R. Das, M. Hicks, Y. Oren, and T. Austin, "ANVIL: Software-Based Protection Against Next-Generation Rowhammer Attacks," in *ASPLOS*, 2016.
- [77] K. Bains *et al.*, "Row Hammer Refresh Command," U.S. Patents: 9,117,544 9,236,110 10,210,925, 2015.
- [78] M. Son, H. Park, J. Ahn, and S. Yoo, "Making DRAM Stronger Against Row Hammering," in *DAC*, 2017.
- [79] S. M. Seyedzadeh, A. K. Jones, and R. Melhem, "Mitigating Wordline Crosstalk Using Adaptive Trees of Counters," in *ISCA*, 2018.
- [80] G. Irazoqui, T. Eisenbarth, and B. Sunar, "MASCAT: Stopping Microarchitectural Attacks Before Execution," *IACR Cryptology*, 2016.
- [81] J. M. You and J.-S. Yang, "MRLoc: Mitigating Row-Hammering Based on Memory Locality," in *DAC*, 2019.
- [82] E. Lee, I. Kang, S. Lee, G. E. Suh, and J. H. Ahn, "TWiCe: Preventing Row-Hammering by Exploiting Time Window Counters," in *ISCA*, 2019.
- [83] Y. Park, W. Kwon, E. Lee, T. J. Ham, J. H. Ahn, and J. W. Lee, "Graphene: Strong yet Lightweight Row Hammer Protection," in *MICRO*, 2020.
- [84] A. G. Yağlıkci, J. S. Kim, F. Devaux, and O. Mutlu, "Security Analysis of the Silver Bullet Technique for RowHammer Prevention," arXiv:2106.07084, 2021.
- [85] A. G. Yağlıkci, M. Patel, J. S. Kim, R. Azizbarzoki, A. Olgun, L. Orosa, H. Hassan, J. Park, K. Kanellopoulos, T. Shahroodi, S. Ghose, and O. Mutlu, "BlockHammer: Preventing RowHammer at Low Cost by Blacklisting Rapidly-Accessed DRAM Rows," in *HPCA*, 2021.
- [86] I. Kang, E. Lee, and J. H. Ahn, "CAT-TWO: Counter-Based Adaptive Tree, Time Window Optimized for DRAM Row-Hammer Prevention," *IEEE Access*, 2020.
- [87] M. Qureshi, A. Rohan, G. Saileshwar, and P. J. Nair, "Hydra: Enabling Low-Overhead Mitigation of Row-Hammer at Ultra-Low Thresholds via Hybrid Tracking," in *ISCA*, 2022.
- [88] G. Saileshwar, B. Wang, M. Qureshi, and P. J. Nair, "Randomized Row-Swap: Mitigating Row Hammer by Breaking Spatial Correlation Between Aggressor and Victim Rows," in *ASPLOS*, 2022.
- [89] R. K. Konoth, M. Oliverio, A. Tatar, D. Andriess, H. Bos, C. Giuffrida, and K. Razavi, "ZebRAM: Comprehensive and Compatible Software Protection Against Rowhammer Attacks," in *OSDI*, 2018.
- [90] S. Vig, S. Bhattacharya, D. Mukhopadhyay, and S.-K. Lam, "Rapid Detection of Rowhammer Attacks Using Dynamic Skewed Hash Tree," in *HASP*, 2018.
- [91] M. J. Kim, J. Park, Y. Park, W. Doh, N. Kim, T. J. Ham, J. W. Lee, and J. H. Ahn, "Mithril: Cooperative Row Hammer Protection on Commodity DRAM Leveraging Managed Refresh," in *HPCA*, 2022.
- [92] G.-H. Lee, S. Na, I. Byun, D. Min, and J. Kim, "CryoGuard: A Near Refresh-Free Robust DRAM Design for Cryogenic Computing," in *ISCA*, 2021.
- [93] M. Marazzi, P. Jattke, F. Solt, and K. Razavi, "REGA: Scalable Rowhammer Mitigation with Refresh-Generating Activations," in *S&P*, 2022.
- [94] Z. Zhang, Y. Cheng, M. Wang, W. He, W. Wang, S. Nepal, Y. Gao, K. Li, Z. Wang, and C. Wu, "SoftTRR: Protect Page Tables against Rowhammer Attacks using Software-only Target Row Refresh," in *USENIX ATC*, 2022.
- [95] B. K. Joardar, T. K. Bletsch, and K. Chakrabarty, "Learning to Mitigate RowHammer Attacks," in *DATE*, 2022.
- [96] J. Juffinger, L. Lamster, A. Kogler, M. Eichlseder, M. Lipp, and D. Gruss, "CSI: Rowhammer-Cryptographic Security and Integrity against Rowhammer," in *S&P*, 2023.
- [97] A. G. Yağlıkci, A. Olgun, M. Patel, H. Luo, H. Hassan, L. Orosa, O. Ergin, and O. Mutlu, "HIRA: Hidden Row Activation for Reducing Refresh Latency of Off-the-Shelf DRAM Chips," in *MICRO*, 2022.
- [98] A. Saxena, G. Saileshwar, P. J. Nair, and M. Qureshi, "AQUA: Scalable Rowhammer Mitigation by Quarantining Aggressor Rows at Runtime," in *MICRO*, 2022.
- [99] S. Enomoto, H. Kuzuno, and H. Yamada, "Efficient Protection Mechanism for CPU Cache Flush Instruction Based Attacks," *IEICE TIS*, 2022.
- [100] E. Manzhosov, A. Hastings, M. Pancholi, R. Piersma, M. T. I. Ziad, and S. Sethumadhavan, "Revisiting Residue Codes for Modern Memories," in *MICRO*, 2022.
- [101] S. M. Ajorpaz, D. Moghimi, J. N. Collins, G. Pokam, N. Abu-Ghazaleh, and D. Tullsen, "EVAX: Towards a Practical, Pro-active & Adaptive Architecture for High Performance & Security," in *MICRO*, 2022.
- [102] A. Naseredini, M. Berger, M. Sammartino, and S. Xiong, "ALARM: Active Learning of Rowhammer Mitigations," <https://users.sussex.ac.uk/~mf21/rh-draft.pdf>, 2022.
- [103] B. K. Joardar, T. K. Bletsch, and K. Chakrabarty, "Machine Learning-based Rowhammer Mitigation," *TCAD*, 2022.
- [104] H. Hassan, A. Olgun, A. G. Yağlıkci, H. Luo, and O. Mutlu, "A Case for Self-Managing DRAM Chips: Improving Performance, Efficiency, Reliability, and Security via Autonomous in-DRAM Maintenance Operations," arXiv:2207.13358, 2022.
- [105] Z. Zhang, Z. Zhan, D. Balasubramanian, B. Li, P. Volgyesi, and X. Koutsoukos, "Leveraging EM Side-Channel Information to Detect Rowhammer Attacks," in *S&P*, 2020.
- [106] K. Loughlin, S. Saroiu, A. Wolman, and B. Kasicki, "Stop! Hammer Time: Rethinking Our Approach to Rowhammer Mitigations," in *HotOS*, 2021.
- [107] F. Devaux and R. Ayrignac, "Method and Circuit for Protecting a DRAM Memory Device from the Row Hammer Effect," U.S. Patent: 10,885,966, 2021.
- [108] J.-W. Han, J. Kim, D. Beery, K. D. Boddag, P. Cuevas, A. Levi, I. Tain, K. Tran, A. J. Walker, S. V. Palayam, A. Arreghini, A. Furnémont, and M. Meyyappan, "Surround

- Gate Transistor With Epitaxially Grown Si Pillar and Simulation Study on Soft Error and Rowhammer Tolerance for DRAM," *IEEE TED*, 2021.
- [109] A. Fakhzadehgan, Y. N. Patt, P. J. Nair, and M. K. Qureshi, "SafeGuard: Reducing the Security Risk from Row-Hammer via Low-Cost Integrity Protection," in *HPCA*, 2022.
- [110] S. Saroiu, A. Wolman, and L. Cojocar, "The Price of Secrecy: How Hiding Internal DRAM Topologies Hurts Rowhammer Defenses," in *IRPS*, 2022.
- [111] S. Saroiu and A. Wolman, "How to Configure Row-Sampling-Based Rowhammer Defenses," *DRAMSec*, 2022.
- [112] K. Loughlin, S. Saroiu, A. Wolman, Y. A. Manerkar, and B. Kasicki, "MOESI-Prime: Preventing Coherence-Induced Hammering in Commodity Workloads," in *ISCA*, 2022.
- [113] R. Zhou, S. Tabrizchi, A. Roohi, and S. Angizi, "LT-PIM: An LUT-Based Processing-in-DRAM Architecture With Rowhammer Self-Tracking," *IEEE CAL*, 2022.
- [114] S. Hong, D. Kim, J. Lee, R. Oh, C. Yoo, S. Hwang, and J. Lee, "DSAC: Low-Cost Rowhammer Mitigation Using In-DRAM Stochastic and Approximate Counting Algorithm," arXiv:2302.03591, 2023.
- [115] M. Marazzi, F. Solt, P. Jattke, K. Takashi, and K. Razavi, "ProTRR: Principled yet Optimal In-DRAM Target Row Refresh," in *S&P*, 2023.
- [116] A. Di Dio, K. Koning, H. Bos, and C. Giuffrida, "Copy-on-Flip: Hardening ECC Memory Against Rowhammer Attacks," in *NDSS*, 2023.
- [117] S. Sharma, D. Sanyal, A. Mukhopadhyay, and R. H. Shaik, "A Review on Study of Defects of DRAM-Rowhammer and Its Mitigation," *Journal For Basic Sciences*, 2022.
- [118] J. Woo, G. Saileshwar, and P. J. Nair, "Scalable and Secure Row-Swap: Efficient and Safe Row Hammer Mitigation in Memory Systems," in *HPCA*, 2023.
- [119] J. H. Park, S. Y. Kim, D. Y. Kim, G. Kim, J. W. Park, S. Yoo, Y.-W. Lee, and M. J. Lee, "Rowhammer Reduction Using a Buried Insulator in a Buried Channel Array Transistor," *IEEE TED*, 2022.
- [120] M. Wi, J. Park, S. Ko, M. J. Kim, N. S. Kim, E. Lee, and J. H. Ahn, "SHADOW: Preventing Row Hammer in DRAM with Intra-Subarray Row Shuffling," in *HPCA*, 2023.
- [121] W. Kim, C. Jung, S. Yoo, D. Hong, J. Hwang, J. Yoon, O. Jung, J. Choi, S. Hyun, M. Kang *et al.*, "A 1.1 V 16Gb DDR5 DRAM with Probabilistic-Aggressor Tracking, Refresh-Management Functionality, Per-Row Hammer Tracking, a Multi-Step Precharge, and Core-Bias Modulation for Security and Reliability Enhancement," in *ISSCC*, 2023.
- [122] C. Gude Ramarao, K. T. Kumar, G. Ujjinappa, and B. V. D. Naidu, "Defending SoCs with FPGAs from Rowhammer Attacks," *Material Science*, 2023.
- [123] K. Guha and A. Chakrabarti, "Criticality based Reliability from Rowhammer Attacks in Multi-User-Multi-FPGA Platform," in *VLSID*, 2022.
- [124] L. France, F. Bruguier, M. Mushtaq, D. Novo, and P. Benoit, "Modeling Rowhammer in the gem5 Simulator," in *CHES*, 2022.
- [125] L. France, F. Bruguier, D. Novo, M. Mushtaq, and P. Benoit, "Reducing the Silicon Area Overhead of Counter-Based Rowhammer Mitigations," in *CryptArch Workshop*, 2022.
- [126] T. Bennett, S. Saroiu, A. Wolman, and L. Cojocar, "Panopticon: A Complete In-DRAM Rowhammer Mitigation," in *DRAMSec*, 2021.
- [127] K. Arikan, A. Palumbo, L. Cassano, P. Revierigo, S. Pontarelli, G. Bianchi, O. Ergin, and M. Ottavi, "Processor Security: Detecting Microarchitectural Attacks via Count-Min Sketches," *VLSI*, 2022.
- [128] C. Tomita, M. Takita, K. Fukushima, Y. Nakano, Y. Shiraishi, and M. Morii, "Extracting the Secrets of OpenSSL with RAMBLED," *Sensors*, 2022.
- [129] A. Saxena, G. Saileshwar, J. Juffinger, A. Kogler, D. Gruss, and M. Qureshi, "PT-Guard: Integrity-Protected Page Tables to Defend Against Breakthrough Rowhammer Attacks," in *DSN*, 2023.
- [130] R. Zhou, S. Ahmed, A. S. Rakin, and S. Angizi, "DNN-Defender: An in-DRAM Deep Neural Network Defense Mechanism for Adversarial Weight Attack," arXiv:2305.08034, 2023.
- [131] S. C. Woo, W. Elsasser, M. Hamburg, E. Linstadt, M. R. Miller, T. Song, and J. Tringali, "RAMPART: Rowhammer Mitigation and Repair for Server Memory Systems," in *MEMSYS*, 2023.
- [132] M. J. Kim, M. Wi, J. Park, S. Ko, J. Choi, H. Nam, N. S. Kim, J. H. Ahn, and E. Lee, "How to Kill the Second Bird with One ECC: The Pursuit of Row Hammer Resilient DRAM," in *MICRO*, 2023.
- [133] A. Olgun, Y. C. Tuğrul, N. Bostanci, I. E. Yüksel, H. Luo, S. Rhyner, A. G. Yağlıkcı, G. F. Oliveira, and O. Mutlu, "ABACuS: All-Bank Activation Counters for Scalable and Low Overhead Rowhammer Mitigation," in *USENIX Security*, 2024.
- [134] A. G. Yağlıkcı, Y. C. Tuğrul, G. F. De Oliveira, I. E. Yüksel, A. Olgun, H. Luo, and O. Mutlu, "Spatial Variation-Aware Read Disturbance Defenses: Experimental Analysis of Real DRAM Chips and Implications on Future Solutions," in *HPCA*, 2024.
- [135] F. N. Bostanci, I. E. Yüksel, A. Olgun, K. Kanellopoulos, Y. C. Tuğrul, A. G. Yağlıcı, M. Sadrosadati, and O. Mutlu, "CoMeT: Count-Min-Sketch-based Row Tracking to Mitigate Rowhammer at Low Cost," in *HPCA*, 2024.
- [136] S. Saroiu, "DDR5 Spec Update Has All It Needs to End Rowhammer: Will It?" <https://stefan.tsk2.com/rh/PRACT/index.html>.
- [137] A. Saxena and M. Qureshi, "STARF: Scalable Tracking for any Rowhammer Threshold," in *HPCA*, 2024.
- [138] JEDEC, *JESD79-5C: DDR5 SDRAM Standard*, 2024.
- [139] O. Canpolat, A. G. Yağlıkcı, G. F. Oliveira, A. Olgun, O. Ergin, and O. Mutlu, "Understanding the Security Benefits and Overheads of Emerging Industry Solutions to DRAM Read Disturbance," in *DRAMSec*, 2024.
- [140] A. Jaleel, G. Saileshwar, S. W. Keckler, and M. Qureshi, "PrIDE: Achieving Secure Rowhammer Mitigation with Low-Cost In-DRAM Trackers," in *ISCA*, 2024.
- [141] A. Saxena, S. Mathur, and M. Qureshi, "Rubix: Reducing the Overhead of Secure Rowhammer Mitigations via Randomized Line-to-Row Mapping," in *ASPLOS*, 2024.
- [142] S. M. Seyedzadeh, A. K. Jones, and R. Melhem, "Counter-Based Tree Structure for Row Hammering Mitigation in DRAM," *CAL*, 2017.
- [143] K. S. Bains and J. B. Halbert, "Row Hammer Monitoring Based on Stored Row Hammer Threshold Value," 2016, U.S. Patent: 9,384,821.
- [144] O. Canpolat, A. G. Yağlıkcı, G. F. Oliveira, A. Olgun, O. Ergin, and O. Mutlu, "Chronus: Understanding and Securing the Cutting-Edge Industry Solutions to DRAM Read Disturbance," in *HPCA*, 2025.
- [145] H. Hassan, A. Olgun, A. G. Yağlıkcı, H. Luo, O. Mutlu, and E. Zurich, "Self-Managing DRAM: A Low-Cost Framework for Enabling Autonomous and Efficient DRAM Maintenance Operations," in *MICRO*, 2024.
- [146] O. Canpolat, A. G. Yağlıkcı, A. Olgun, I. E. Yüksel, Y. C. Tuğrul, K. Kanellopoulos, O. Ergin, and O. Mutlu, "BreakHammer: Enhancing Rowhammer Mitigations by Carefully Throttling Suspect Threads," in *MICRO*, 2024.
- [147] D. S. Yaney, C.-Y. Lu, R. A. Kohler, M. J. Kelly, and J. T. Nelson, "A Meta-Stable Leakage Phenomenon in DRAM Charge Storage-Variable Hold Time," in *IEDM*, 1987.
- [148] Restle, Park, and Lloyd, "DRAM Variable Retention Time," in *IEDM*, 1992.
- [149] J. Liu, B. Jaiyen, Y. Kim, C. Wilkerson, O. Mutlu, J. Liu, B. Jaiyen, Y. Kim, C. Wilkerson, and O. Mutlu, "An Experimental Study of Data Retention Behavior in Modern DRAM Devices," in *ISCA*, 2013.
- [150] U. Kang, H.-S. Yu, C. Park, H. Zheng, J. Halbert, K. Bains, S. Jang, and J. S. Choi, "Co-Architecting Controllers and DRAM to Enhance DRAM Process Scaling," in *The Memory Forum*, 2014.
- [151] S. Khan, D. Lee, Y. Kim, A. R. Alameldeen, C. Wilkerson, and O. Mutlu, "The Efficacy of Error Mitigation Techniques for DRAM Retention Failures: a Comparative Experimental Study," in *SIGMETRICS*, 2014.
- [152] Y. Mori, K. Ohyu, K. Okonogi, and R.-I. Yamada, "The Origin of Variable Retention Time in DRAM," in *IEDM*, 2005.
- [153] M. K. Qureshi, D.-H. Kim, S. Khan, P. J. Nair, and O. Mutlu, "AVATAR: A Variable-Retention-Time (VRT) Aware Refresh for DRAM Systems," in *DSN*, 2015.
- [154] J. Kim, M. Sullivan, and M. Erez, "Bamboo ECC: Strong, Safe, and Flexible Codes for Reliable Computer Memory," in *HPCA*, 2015.
- [155] AMD, "BIOS and Kernel Developer's Guide (BKDG) for AMD Family 15h Models 00h-0fh Processors," Developer's Guide, 2013.
- [156] R. Yeleswarapu and A. K. Somani, "Addressing Multiple Bit/Symbol Errors in DRAM Subsystem," arXiv:1908.01806, 2020.
- [157] C. L. Chen, "Symbol Error Correcting Codes for Memory Applications," in *Annual Symposium on Fault Tolerant Computing*, 1996.
- [158] JEDEC, *JESD209-5A: LPDDR5 SDRAM Standard*, 2020.
- [159] JEDEC, *JESD209-4B: Low Power Double Data Rate 4 (LPDDR4) Standard*, 2017.
- [160] JEDEC, *JESD79F: Double Data Rate (DDR) SDRAM Standard*, 2008.
- [161] JEDEC, *JESD79-4C: DDR4 SDRAM Standard*, 2020.
- [162] JEDEC, *JESD79-3: DDR3 SDRAM Standard*, 2012.
- [163] JEDEC, *JESD235D: High Bandwidth Memory DRAM (HBM1, HBM2)*, 2021.
- [164] Micron, *SDRAM, 4Gb: x4, x8, x16 DDR4 SDRAM Features*, 2014.
- [165] J. S. Kim, M. Patel, A. G. Yağlıkcı, H. Hassan, R. Azizi, L. Orosa, and O. Mutlu, "Revisiting Rowhammer: An Experimental Analysis of Modern Devices and Mitigation Techniques," in *ISCA*, 2020.
- [166] L. Orosa, A. G. Yağlıkcı, H. Luo, A. Olgun, J. Park, H. Hassan, M. Patel, J. S. Kim, and O. Mutlu, "A Deeper Look into Rowhammer's Sensitivities: Experimental Analysis of Real DRAM Chips and Implications on Future Attacks and Defenses," in *MICRO*, 2021.
- [167] A. G. Yağlıkcı, H. Luo, G. F. De Oliveira, A. Olgun, M. Patel, J. Park, H. Hassan, J. S. Kim, L. Orosa, and O. Mutlu, "Understanding Rowhammer Under Reduced Wordline Voltage: An Experimental Study Using Real DRAM Devices," in *DSN*, 2022.
- [168] H. Hassan, M. Patel, J. S. Kim, A. G. Yağlıkcı, N. Vijaykumar, N. Mansouri Ghiasi, S. Ghose, and O. Mutlu, "CROW: A Low-Cost Substrate for Improving DRAM Performance, Energy Efficiency, and Reliability," in *ISCA*, 2019.
- [169] K. Park, D. Yun, and S. Baeg, "Statistical Distributions of Row-hammering Induced Failures in DDR3 Components," *Microelectronics Reliability*, 2016.
- [170] K. Park, C. Lim, D. Yun, and S. Baeg, "Experiments and Root Cause Analysis for Active-precharge Hammering Fault in DDR3 SDRAM under 3x nm Technology," *Microelectronics Reliability*, 2016.
- [171] C. Lim, K. Park, and S. Baeg, "Active Precharge Hammering to Monitor Displacement Damage Using High-Energy Protons in 3x-nm SDRAM," *TNS*, 2017.
- [172] S.-W. Ryu, K. Min, J. Shin, H. Kwon, D. Nam, T. Oh, T.-S. Jang, M. Yoo, Y. Kim, and S. Hong, "Overcoming the Reliability Limitation in the Ultimately Scaled DRAM using Silicon Migration Technique by Hydrogen Annealing," in *IEDM*, 2017.
- [173] C. Lim, K. Park, G. Bak, D. Yun, M. Park, S. Baeg, S.-J. Wen, and R. Wong, "Study of Proton Radiation Effect to Row Hammer Fault in DDR4 SDRAMs," *Microelectronics Reliability*, 2018.
- [174] D. Yun, M. Park, C. Lim, and S. Baeg, "Study of TID Effects on One Row Hammering using Gamma in DDR4 SDRAMs," in *IRPS*, 2018.
- [175] T. Yang and X.-W. Lin, "Trap-Assisted DRAM Row Hammer Effect," *EDL*, 2019.
- [176] A. J. Walker, S. Lee, and D. Beery, "On DRAM Rowhammer and the Physics on Insecurity," *IEEE TED*, 2021.
- [177] M. N. I. Khan and S. Ghosh, "Analysis of Row Hammer Attack on STTRAM," in *ICCD*, 2018.
- [178] S. Agarwal, H. Dixit, D. Datta, M. Tran, D. Houssameddine, D. Shum, and F. Benistant, "Rowhammer for Spin Torque based Memory: Problem or not?" in *INTERMAG*, 2018.
- [179] H. Li, H.-Y. Chen, Z. Chen, B. Chen, R. Liu, G. Qiu, P. Huang, F. Zhang, Z. Jiang, B. Gao, L. Liu, X. Liu, S. Yu, H.-S. P. Wong, and J. Kang, "Write Disturb Analyses on Half-Selected Cells of Cross-Point RRAM Arrays," in *IRPS*, 2014.
- [180] K. Ni, X. Li, J. A. Smith, M. Jerry, and S. Datta, "Write Disturb in Ferroelectric FETs and Its Implication for 1T-FeFET AND Memory Arrays," *IEEE EDL*, 2018.
- [181] P. R. Genssler, V. M. van Santen, J. Henkel, and H. Amrouch, "On the Reliability of FeFET On-Chip Memory," *TC*, 2022.

- [182] W. He, Z. Zhang, Y. Cheng, W. Wang, W. Song, Y. Gao, Q. Zhang, K. Li, D. Liu, and S. Nepal, "WhistleBlower: A System-level Empirical Study on RowHammer," *TC*, 2023.
- [183] S. Baeg, D. Yun, M. Chun, and S.-J. Wen, "Estimation of the Trap Energy Characteristics of Row Hammer-Affected Cells in Gamma-Irradiated DDR4 DRAM," *IEEE Transactions on Nuclear Science*, 2022.
- [184] O. Mutlu, "RowHammer," <https://people.inf.ethz.ch/omutlu/pub/onur-Rowhammer-TopPicksinHardwareEmbeddedSecurity-November-8-2018.pdf>, 2018, Top Picks in Hardware and Embedded Security.
- [185] A. Olgun, M. Osseiran, A. G. Yaglikci, Y. C. Tuğrul, H. Luo, S. Rhyner, B. Salami, J. Gomez Luna, and O. Mutlu, "An Experimental Analysis of RowHammer in HBM2 DRAM Chips," in *DSN Disrupt*, 2023.
- [186] A. Olgun, H. Hassan, A. G. Yağlıkci, Y. C. Tuğrul, L. Orosa, H. Luo, M. Patel, E. Oğuz, and O. Mutlu, "DRAM Bender: An Extensible and Versatile FPGA-based Infrastructure to Easily Test State-of-the-art DRAM Chips," *TCAD*, 2023.
- [187] L. Zhou, J. Li, Z. Qiao, P. Ren, Z. Sun, J. Wang, B. Wu, Z. Ji, R. Wang, K. Cao, and R. Huang, "Double-sided Row Hammer Effect in Sub-20 nm DRAM: Physical Mechanism, Key Features and Mitigation," in *IRPS*, 2023.
- [188] SAFARI Research Group, "DRAM Bender — GitHub Repository," <https://github.com/CMU-SAFARI/DRAM-Bender>, 2022.
- [189] H. Hassan, N. Vijaykumar, S. Khan, S. Ghose, K. Chang, G. Pekhimenko, D. Lee, O. Ergin, and O. Mutlu, "SoftMC: A Flexible and Practical Open-Source Infrastructure for Enabling Experimental DRAM Studies," in *HPCA*, 2017.
- [190] SAFARI Research Group, "SoftMC — GitHub Repository," <https://github.com/CMU-SAFARI/SoftMC>, 2017.
- [191] AMD Xilinx, "AMD Xilinx Alveo U200 FPGA Board," <https://www.xilinx.com/products/boards-and-kits/alveo/u200.html>.
- [192] AMD Xilinx, "AMD Xilinx Alveo U50 FPGA Board," <https://www.amd.com/en/products/accelerators/alveo/u50/a-u50-p00g-pq-g.html>.
- [193] Bittware, "Bittware XUPVH FPGA Board," <https://www.bittware.com/fpga/xup-vvh/>.
- [194] Maxwell, "FT20X User Manual," <https://www.maxwell-fa.com/upload/files/base/8/m/311.pdf>.
- [195] M. Patel, J. S. Kim, and O. Mutlu, "The Reach Profiler (REAPER): Enabling the Mitigation of DRAM Retention Failures via Profiling at Aggressive Conditions," in *ISCA*, 2017.
- [196] Micron, *16Gb: x4, x8, x16 DDR4 SDRAM Features - MT40A4G4, MT40A2G8, MT40A1G16*, 2018.
- [197] M. Patel, J. Kim, T. Shahroodi, H. Hassan, and O. Mutlu, "Bit-Exact ECC Recovery (BEER): Determining DRAM On-Die ECC Functions by Exploiting DRAM Data Retention Characteristics," in *MICRO*, 2020.
- [198] M. Patel, G. F. de Oliveira Jr., and O. Mutlu, "HARP: Practically and Effectively Identifying Uncorrectable Errors in Main Memory Chips That Use On-Die ECC," in *MICRO*, 2021.
- [199] R. T. Smith, J. D. Chlipala, J. F. Bindels, R. G. Nelson, F. H. Fischer, and T. F. Mantz, "Laser Programmable Redundancy and Yield Improvement in a 64K DRAM," *JSSC*, 1981.
- [200] M. Horiguchi, "Redundancy Techniques for High-Density DRAMs," in *ISIS*, 1997.
- [201] B. Keeth and R. Baker, *DRAM Circuit Design: A Tutorial*. Wiley, 2001.
- [202] K. Itoh, *VLSI Memory Chip Design*. Springer, 2001.
- [203] V. Seshadri, T. Mullins, A. Boroumand, O. Mutlu, P. B. Gibbons, M. A. Kozuch, and T. C. Mowry, "Gather-Scatter DRAM: In-DRAM Address Translation to Improve the Spatial Locality of Non-Unit Strided Accesses," in *MICRO*, 2015.
- [204] S. Khan, D. Lee, and O. Mutlu, "PARBOR: An Efficient System-Level Technique to Detect Data-Dependent Failures in DRAM," in *DSN*, 2016.
- [205] S. Khan, C. Wilkerson, Z. Wang, A. R. Alameldeen, D. Lee, and O. Mutlu, "Detecting and Mitigating Data-Dependent DRAM Failures by Exploiting Current Memory Content," in *MICRO*, 2017.
- [206] D. Lee, S. Khan, L. Subramanian, S. Ghose, R. Ausavarungnirun, G. Pekhimenko, V. Seshadri, and O. Mutlu, "Design-induced Latency Variation in Modern DRAM Chips: Characterization, Analysis, and Latency Reduction Mechanisms," *POMACS*, 2017.
- [207] A. van de Goor and I. Schanstra, "Address and Data Scrambling: Causes and Impact on Memory Tests," in *DELTA*, 2002.
- [208] K. Pearson, "On the criterion that a given system of deviations from the probable in the case of a correlated system of variables is such that it can be reasonably supposed to have arisen from random sampling," *Philosophical magazine*, vol. 50, no. 302, 1900.
- [209] P. J. Brockwell, *Time Series: Theory and Methods*. Springer-Verlag, 1991.
- [210] L. Zhou, J. Li, P. Ren, S. Ye, D. Wang, Z. Qiao, and Z. Ji, "Understanding the Physical Mechanism of RowPress at the Device-Level in Sub-20 nm DRAM," in *IRPS*, 2024.
- [211] L. Zhou, S. Ye, R. Wang, and Z. Ji, "Unveiling RowPress in Sub-20 nm DRAM Through Comparative Analysis With Row Hammer: From Leakage Mechanisms to Key Features," in *IEEE TED*, 2024.
- [212] B. Oh, H.-J. Cho, H. Kim, Y. Son, T. Kang, S. Park, S. Jang, J.-H. Lee, and H. Shin, "Characterization of an Oxide Trap Leading to Random Telegraph Noise in Gate-Induced Drain Leakage Current of DRAM Cell Transistors," *IEEE TED*, 2011.
- [213] Y. Sun, X. Liu, N. Wang, J. Jeon, B. Wu, and K. Cao, "Trap-Assisted Passing Word Line Leakage and Variable Retention Time in DRAM," in *IEEE ICET*, 2021.
- [214] M. Patel, J. S. Kim, H. Hassan, and O. Mutlu, "Understanding and Modeling On-Die Error Correction in Modern DRAM: An Experimental Study Using Real Devices," in *DSN*, 2019.
- [215] K. Kraft, C. Sudarshan, D. M. Mathew, C. Weis, N. Wehn, and M. Jung, "Improving the Error Behavior of DRAM by Exploiting its Z-Channel Property," in *DATE*, 2018.
- [216] IEEE Electronics Packaging Society, "Heterogeneous Integration Roadmap, Chapter 17: Test Technology," https://eps.ieee.org/images/files/HIR_2019/HIR1_ch17_test.pdf, 2019.
- [217] A. van de Goor, "An Industrial Evaluation of DRAM Tests," *IEEE Design & Test of Computers*, 2004.
- [218] M. Qureshi, S. Qazi, and A. Jaleel, "MINT: Securely Mitigating Rowhammer with a Minimalist In-DRAM Tracker," arXiv:2407.16038 [cs.CR], 2024.
- [219] SAFARI Research Group, "Ramulator 2.0 — GitHub Repository," <https://github.com/CMU-SAFARI/ramulator2>, 2023.
- [220] H. Luo, Y. Tuğrul, F. Bostanc, A. Olgun, A. Yağlıkci, and O. Mutlu, "Ramulator 2.0: A Modern, Modular, and Extensible DRAM Simulator," *IEEE CAL*, 2024.
- [221] SAFARI Research Group, "Ramulator — GitHub Repository," <https://github.com/CMU-SAFARI/ramulator>, 2021.
- [222] Y. Kim *et al.*, "Ramulator: A Fast and Extensible DRAM Simulator," *CAL*, 2016.
- [223] Standard Performance Evaluation Corp., "SPEC CPU 2006," <http://www.spec.org/cpu2006/>, 2006.
- [224] Standard Performance Evaluation Corp., "SPEC CPU 2017," <http://www.spec.org/cpu2017/>, 2017.
- [225] Transaction Processing Performance Council, "TPC Benchmarks," <http://tpc.org/>.
- [226] J. E. Fritts *et al.*, "MediaBench II Video: Expediting the next Generation of Video Systems Research," *Microprocess. Microsyst.*, 2009.
- [227] B. Cooper *et al.*, "Benchmarking Cloud Serving Systems with YCSB," in *SoCC*, 2010.
- [228] K. K. Chang, A. Kashyap, H. Hassan, S. Ghose, K. Hsieh, D. Lee, T. Li, G. Pekhimenko, S. Khan, and O. Mutlu, "Understanding Latency Variation in Modern DRAM Chips: Experimental Characterization, Analysis, and Optimization," in *SIGMETRICS*, 2016.
- [229] J. Liu, B. Jaiyen, R. Veras, and O. Mutlu, "RAIDR: Retention-Aware Intelligent DRAM Refresh," in *ISCA*, 2012.
- [230] S. Baek, S. Cho, and R. Melhem, "Refresh Now and Then," *IEEE TC*, 2014.
- [231] J. Wang, X. Dong, and Y. Xie, "ProactiveDRAM: A DRAM-initiated Retention Management Scheme," in *ICCD*, 2014.
- [232] C.-H. Lin, D.-Y. Shen, Y.-J. Chen, C.-L. Yang, and M. Wang, "SECRET: Selective Error Correction for Refresh Energy reduction in DRAMs," in *ICCD*, 2012.
- [233] P. J. Nair, D.-H. Kim, and M. K. Qureshi, "ArchShield: Architectural Framework for Assisting DRAM Scaling by Tolerating High Error Rates," in *ISCA*, 2013.
- [234] A. Das, H. Hassan, and O. Mutlu, "VRL-DRAM: Improving DRAM Performance via Variable Refresh Latency," in *DAC*, 2018.
- [235] M. Qureshi, "Rethinking ECC in the Era of Row-Hammer," in *DRAMSec*, 2021.
- [236] Z. Lang, P. Jattke, M. Marazzi, and K. Razavi, "BLASTER: Characterizing the Blast Radius of Rowhammer," in *DRAMSec*, 2023.
- [237] H. Nam, S. Baek, M. Wi, M. J. Kim, J. Park, C. Song, N. S. Kim, and J. H. Ahn, "DRAMScope: Uncovering DRAM Microarchitecture and Characteristics by Issuing Memory Commands," in *ISCA*, 2024.
- [238] H. Nam, S. Baek, M. Wi, M. J. Kim, J. Park, C. Song, N. S. Kim, and J. H. Ahn, "X-ray: Discovering DRAM Internal Structure and Error Characteristics by Issuing Memory Commands," *IEEE CAL*, 2023.
- [239] M. Farmani, M. Tehranipoor, and F. Rahman, "RHAT: Efficient RowHammer-aware test for modern DRAM modules," in *ETS*, 2021.
- [240] Z. Zhang, W. He, Y. Cheng, W. Wang, Y. Gao, M. Wang, K. Li, S. Nepal, and Y. Xiang, "BitMine: An End-to-End Tool for Detecting RowHammer Vulnerability," *IEEE TIFS*, 2021.
- [241] PassMark Software, "MemTest86 (Version 6.2 and later) [Computer software]," <https://www.memtest86.com/>.
- [242] O. Mutlu, "Retrospective: Flipping Bits in Memory Without Accessing Them: An Experimental Study of DRAM Disturbance Errors," arXiv:2306.16093 [cs.CR], 2023.
- [243] Micron, *16Gb DDR5 SDRAM Addendum MT60B4G4, MT60B2G8, MT60B1G16 Die Revision A*, 2021.

Appendix

A. Read Disturbance Threshold Testing

We describe a methodology for estimating the read disturbance threshold (RDT) testing time and energy consumption for a double-sided RowHammer access pattern (i.e., t_{AggOn} = minimum t_{RAS}). We use the methodology to demonstrate testing time and energy consumption for a DRAM row, a bank of rows, multiple banks, and a DRAM module, for a varying number of test iterations. An iteration of an RDT test yields one RDT measurement for one DRAM row and consists of 1) initializing the victim row and the two aggressor rows, 2) performing double-sided RowHammer by repeatedly activating the aggressor rows, and 3) reading victim row's data to check for bitflips. To estimate RDT testing times, we tightly schedule the DRAM commands needed to perform each step. To estimate energy consumption, we use the current values reported in [243]. We report both 1) the number and order of the DRAM commands needed to perform the RDT test (Tables 4 and 5), and 2) the time required to perform the RDT test using the timing parameters provided by the DDR5 standard [138] (Table 6) assuming 8800 MT/s speed rate.

Table 4: List of DRAM commands issued to measure RDT once for one victim DRAM row in one bank using the double-sided read disturbance access pattern [1, 16, 165, 166] (one hammer constitutes activation of the two aggressor rows)

Command	Address	Timing	# of Commands
ACT	Victim	t_{RCD}	1
WRITE		$t_{CCD_L_WR}$	127
		t_{WR}	1
PRE		t_{RP}	1
ACT	Aggressor 1	t_{RCD}	1
WRITE		$t_{CCD_L_WR}$	127
		t_{WR}	1
PRE		t_{RP}	1
ACT	Aggressor 2	t_{RCD}	1
WRITE		$t_{CCD_L_WR}$	127
		t_{WR}	1
PRE		t_{RP}	1
ACT	Aggressor 1	t_{AggOn}	# of hammers
PRE		t_{RP}	
ACT	Aggressor 2	t_{AggOn}	
PRE		t_{RP}	
ACT	Victim	t_{RCD}	1
		t_{CCD_L}	127
READ		t_{RTP}	1

Table 5: List of DRAM commands issued to simultaneously (as much as possible, obeying timing constraints) measure RDT once for one victim DRAM row address across 16 banks using the double-sided read disturbance access pattern [1, 16, 165, 166] (one hammer constitutes activation of two aggressor row addresses in 16 banks)

Command	Address	Timing	# of Commands
ACT	Victim	t_{RRD_S}	16
WRITE		t_{CCD_S}	2032
		t_{WR}	1
PRE		t_{RP}	1
ACT	Aggressor 1	t_{RRD_S}	16
WRITE		t_{CCD_S}	2032
		t_{WR}	1
PRE		t_{RP}	1
ACT	Aggressor 2	t_{RRD_S}	16
WRITE		t_{CCD_S}	2032
		t_{WR}	1
PRE		t_{RP}	1
ACT	Aggressor 1	$\text{Max}(t_{AggOn}, t_{RRD_S} * 16)$	# of hammers
PRE		t_{RP}	
ACT	Aggressor 2	$\text{Max}(t_{AggOn}, t_{RRD_S} * 16)$	
PRE		t_{RP}	
ACT	Victim	t_{RCD}	1
		t_{CCD_L}	127
READ		t_{RTP}	1

Table 6: DRAM timing parameters used in our analysis and their values (in nanoseconds) as depicted in the JEDEC DDR5 standard [138]

Timing Parameter	Latency (nanoseconds)
tRRD_S	1.816
tCCD_S	1.816
tCCD_L	5.000
tCCD_L_WR	20.000
tRCD	14.090
tRP	14.090
tRAS	32.000
tRTP	7.500
tWR	30.000

Analysis Summary. Even if we test only for RowHammer using *only* a single data pattern and a single temperature level, i.e., using $t_{AggOn} = t_{RAS}$ and a hammer count of 1K, testing an entire DRAM chip with 32 banks for 100K RDT measurements for each row takes 61 days and consumes 13 megajoules (as shown in Fig. 20a and Fig. 20b). If we test for longer, the testing time and energy consumption would scale linearly. Increasing the data patterns and temperature levels would increase testing time linearly with each factor. Testing for RowPress (with $t_{AggOn} = 7.8\mu s$ and hammer count = 1K) would increase the time to 13 years and consume 95 megajoules (as shown in Fig. 24a and Fig. 24b).

Even if we make *only* 1K RDT measurements per row, testing an entire DRAM chip with 32 banks for RowHammer (using $t_{AggOn} = t_{RAS}$ and a hammer count of 1K) takes 15 hours and consumes 128 kilojoules (as shown in Fig. 19a and Fig. 19b). Testing for RowPress (with $t_{AggOn} = 7.8\mu s$) would increase the time to 48 days and consume 950 kilojoules (as shown in Fig. 23a and Fig. 23b).

§A.1 and §A.2 provide detailed information on the testing time and energy consumption using different test parameters (e.g., hammer count, number of rows in a DRAM bank, and number of simultaneously tested DRAM banks) for RowHammer ($t_{AggOn} = t_{RAS}$) and RowPress ($t_{AggOn} = 7.8\mu s$), respectively.

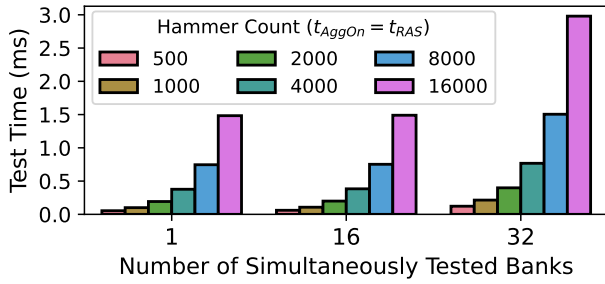
A.1. RowHammer Testing Time and Energy Consumption

Figure 17a and 17b respectively show the time (in milliseconds, y-axis) and energy (in millijoules) to perform one RDT measurement for a victim row for a varying number of hammer counts (different colored bars) and varying number of simultaneously tested DRAM banks (x-axis) for $t_{AggOn} = t_{RAS}$.

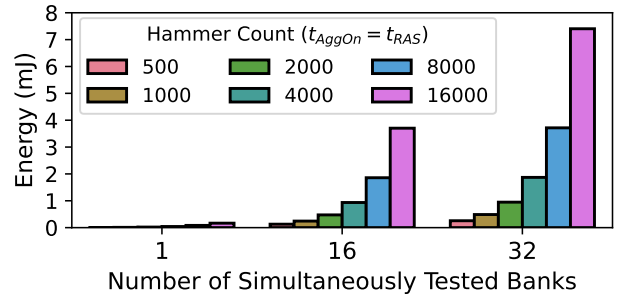
Figure 18 shows the time (in seconds, y-axis) to perform one RDT measurement for a victim row for a varying number of hammer counts (different colored bars) and varying number of DRAM rows in a bank (x-axis) for $t_{AggOn} = t_{RAS}$.

Figure 19a and 19b respectively show the time (in hours, y-axis) and energy (in kilojoules) to perform 1K RDT measurements for number of hammers = 1K, for a varying number of victim rows (different colored bars) and simultaneously tested DRAM banks (x-axis) for $t_{AggOn} = t_{RAS}$.

Figure 20a and 20b respectively show the time (in days, y-axis) and energy (in kilojoules) to perform 100K RDT measurements for number of hammers = 1K, for a varying number of victim rows (different colored bars) and simultaneously tested DRAM banks (x-axis) for $t_{AggOn} = t_{RAS}$.



(a) Time to perform a single RDT measurement for a single victim row for a varying number of hammer counts and varying number of simultaneously (as much as possible, obeying timing constraints) tested DRAM banks



(b) Energy to perform a single RDT measurement for a single victim row for a varying number of hammer counts and varying number of simultaneously (as much as possible, obeying timing constraints) tested DRAM banks

Figure 17: RowHammer testing time and energy consumption for a single RDT measurement

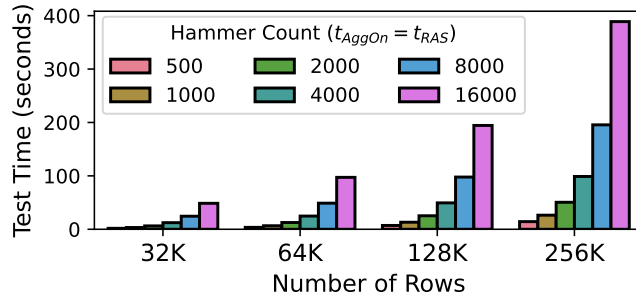
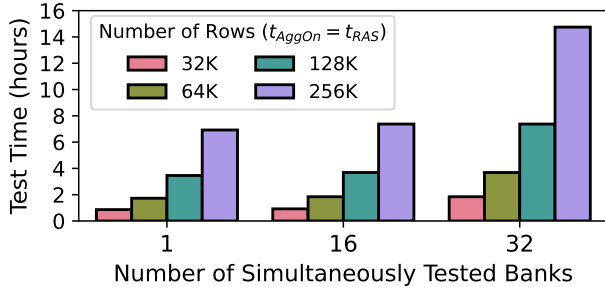
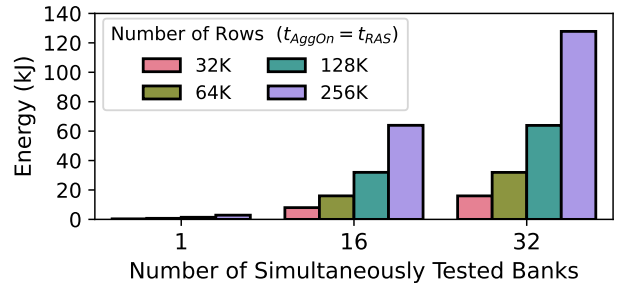


Figure 18: Time to perform a single RDT measurement for a given number of victim rows (x-axis) and a varying number of hammer counts (# of hammers) in a single DRAM bank

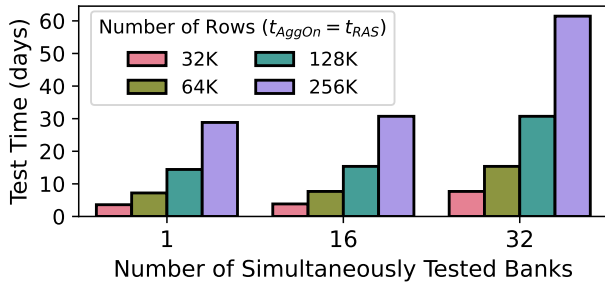


(a) Time to perform 1K RDT measurements for a varying number of victim rows and simultaneously (as much as possible, obeying timing constraints) tested DRAM banks given number of hammers = 1K

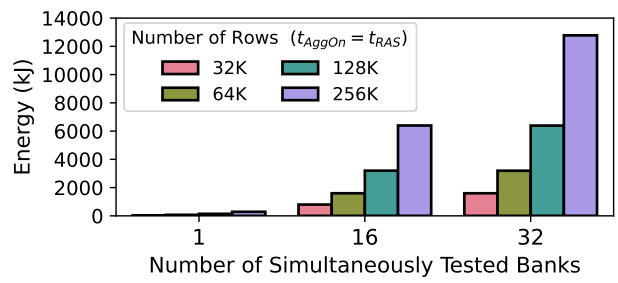


(b) Energy to perform 1K RDT measurements for a varying number of victim rows and simultaneously (as much as possible, obeying timing constraints) tested DRAM banks given number of hammers = 1K

Figure 19: RowHammer testing time and energy consumption for 1K RDT measurements



(a) Time to perform 100K RDT measurements for a varying number of victim rows and simultaneously (as much as possible, obeying timing constraints) tested DRAM banks given number of hammers = 1K



(b) Energy to perform 100K RDT measurements for a varying number of victim rows and simultaneously (as much as possible, obeying timing constraints) tested DRAM banks given number of hammers = 1K

Figure 20: RowHammer testing time and energy consumption for 100K RDT measurements

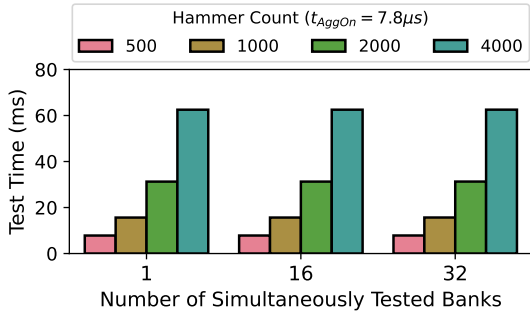
A.2. RowPress Testing Time and Energy Consumption

Figure 21a and 21b respectively show the time (in milliseconds, y-axis) and energy (in millijoules) to perform one RDT measurement for a victim row for a varying number of hammer counts (different colored bars) and varying number of simultaneously tested DRAM banks (x-axis) for $t_{AggOn} = 7.8\mu s$.

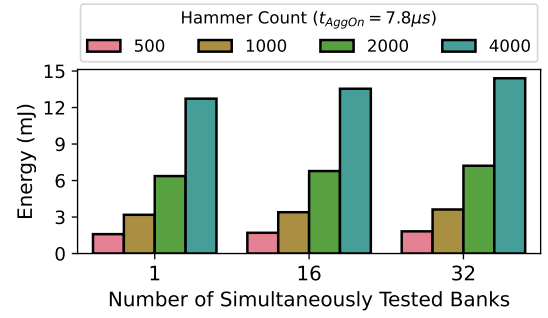
Figure 22 shows the time (in seconds, y-axis) to perform one RDT measurement for a victim row for a varying number of hammer counts (different colored bars) and varying number of DRAM rows in a bank (x-axis) for $t_{AggOn} = 7.8\mu s$.

Figure 23a and 23b respectively show the time (in hours, y-axis) and energy (in kilojoules) to perform 1K RDT measurements for number of hammers = 1K, for a varying number of victim rows (different colored bars) and simultaneously tested DRAM banks (x-axis) for $t_{AggOn} = 7.8\mu s$.

Figure 24a and 24b respectively show the time (in days, y-axis) and energy (in kilojoules) to perform 100K RDT measurements for number of hammers = 1K, for a varying number of victim rows (different colored bars) and simultaneously tested DRAM banks (x-axis) for $t_{AggOn} = 7.8\mu s$.



(a) Time to perform a single RDT measurement for a single victim row for a varying number of hammer counts and varying number of simultaneously (as much as possible, obeying timing constraints) tested DRAM banks



(b) Energy to perform a single RDT measurement for a single victim row for a varying number of hammer counts and varying number of simultaneously (as much as possible, obeying timing constraints) tested DRAM banks

Figure 21: RowPress testing time and energy consumption for a single RDT measurement

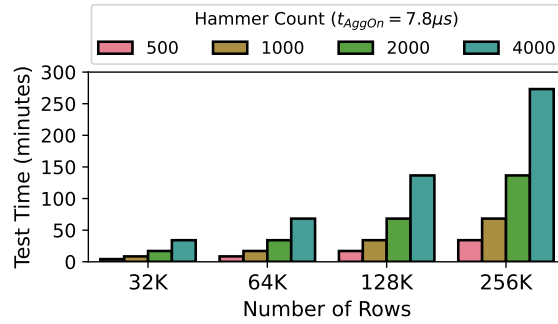
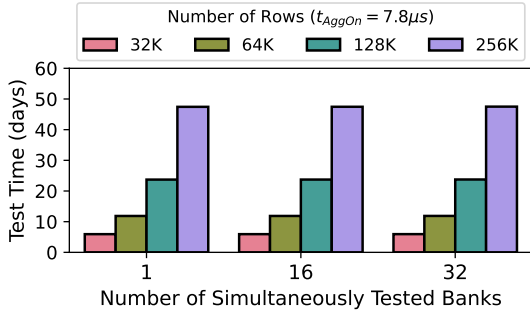
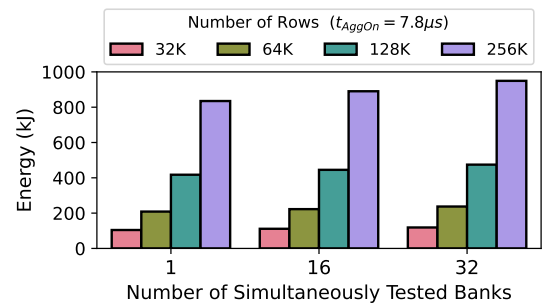


Figure 22: Time to perform a single RDT measurement for a given number of victim rows (x-axis) and a varying number of hammer counts (# of hammers) in a single DRAM bank

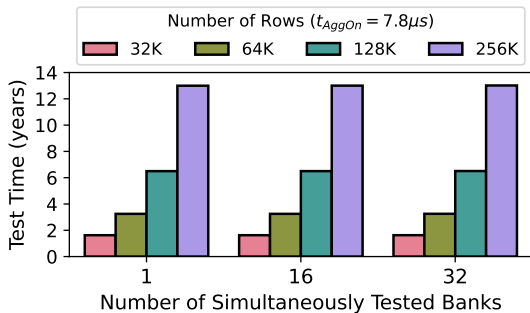


(a) Time to perform 1K RDT measurements for a varying number of victim rows and simultaneously (as much as possible, obeying timing constraints) tested DRAM banks given number of hammers = 1K

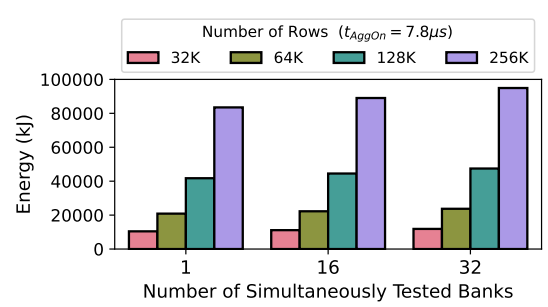


(b) Energy to perform 1K RDT measurements for a varying number of victim rows and simultaneously (as much as possible, obeying timing constraints) tested DRAM banks given number of hammers = 1K

Figure 23: RowPress testing time and energy consumption for 1K RDT measurements



(a) Time to perform 100K RDT measurements for a varying number of victim rows and simultaneously (as much as possible, obeying timing constraints) tested DRAM banks given number of hammers = 1K



(b) Energy to perform 100K RDT measurements for a varying number of victim rows and simultaneously (as much as possible, obeying timing constraints) tested DRAM banks given number of hammers = 1K

Figure 24: RowPress testing time and energy consumption for 100K RDT measurements

B. Detailed Information on Tested DDR4 Modules and HBM2 Chips

Table 7 shows the detailed information on the 21 tested DDR4 modules and 4 HBM2 Chips. We provide the expected normalized value of the minimum RDT across 1K measurements (defined in §5) for the median and the worst-case DRAM row in each tested module for varying number of measurements ($N = 1, 5, 50, \text{ and } 500$).

Table 7: 21 DDR4 modules and 4 HBM2 chips that we characterize in this work. For each module, we 1) provide the median and maximum expected normalized value of the minimum RDT across 1,000 RDT measurements (see §5) across all tested DRAM rows and combinations of test parameters, and 2) the minimum observed RDT across all measurements, tested DRAM rows, and combinations of test parameters for $t_{\text{AggOn}} = t_{\text{RAS}}$ and $t_{\text{AggOn}} = t_{\text{REFI}}$.

Module	Module Identifier	Chip Identifier	Bandwidth	Organization				Expected Normalized Value of the Minimum RDT Across 1,000 Measurements								Minimum Observed RDT	
								N = 1		N = 5		N = 50		N = 500			
				Size (GB)	Ranks	Chips	Pins	Median	Max	Median	Max	Median	Max	Median	Max	$t_{\text{AggOn}} = t_{\text{RAS}}$	$t_{\text{AggOn}} = t_{\text{REFI}}$
H0	Unknown ^a	H5AN8G8NJJR-VKC	2666 MT/s	16	2	8	x8	1.04	1.59	1.03	1.47	1.01	1.28	1.00	1.10	23238	9436
H1	HMAA4GU7CJR8N-XN	H5ANAG8NCJR-XNC	3200 MT/s	32	2	8	x8	1.07	1.51	1.04	1.46	1.02	1.31	1.00	1.12	7835	1941
H2	HMA81GU7AFR8N-UH	H5AN8G8NAFR-UHC	2400 MT/s	8	1	8	x8	1.05	1.35	1.03	1.33	1.02	1.27	1.00	1.10	25606	12143
H3	HMA81GU7DJR8N-WM	H5AN8G8NDJR-WMC	2933 MT/s	8	1	8	x8	1.05	1.54	1.04	1.51	1.02	1.37	1.00	1.09	9804	4185
H4	HMA81GU7DJR8N-WM	H5AN8G8NDJR-WMC	2933 MT/s	8	1	8	x8	1.05	1.63	1.04	1.54	1.02	1.41	1.00	1.12	10750	2941
H5	KSM26ES8/8HD	H5AN8G8NDJR-XNC	3200 MT/s	8	1	8	x8	1.05	1.56	1.03	1.52	1.02	1.35	1.00	1.13	13572	3185
H6	KSM26ES8/8HD	H5AN8G8NDJR-XNC	3200 MT/s	8	1	8	x8	1.05	1.70	1.03	1.67	1.02	1.54	1.00	1.28	9680	3770
M0	MTA4ATF1G64HZ-3G2E1	MT40A1G16KD-062E:E	3200 MT/s	8	1	4	x16	1.06	1.45	1.04	1.35	1.02	1.21	1.00	1.07	4980	2025
M1	MTA18ASF4G72HZ-3G2F1Z1	MT40A2G8SA-062E:F	3200 MT/s	32	2	8	x8	1.08	1.78	1.05	1.70	1.03	1.40	1.00	1.10	4250	1796
M2	MTA18ASF4G72HZ-3G2F1Z1	MT40A2G8SA-062E:F	3200 MT/s	32	2	8	x8	1.08	1.47	1.06	1.41	1.03	1.28	1.00	1.08	4741	1620
M3	KSM32ES8/8MR	Unknown ^a	3200 MT/s	8	1	8	x8	1.08	1.46	1.05	1.40	1.03	1.24	1.01	1.06	4691	1788
M4	KSM32ES8/8MR	Unknown ^a	3200 MT/s	8	1	8	x8	1.08	1.84	1.05	1.74	1.03	1.42	1.01	1.18	3686	2320
M5	KSM32SED8/16MR	MT40A1G8SA-062E:R	3200 MT/s	16	2	8	x8	1.08	1.83	1.05	1.51	1.03	1.35	1.01	1.13	4675	2177
M6	KSM32ES8/16MF	MT40A2G8SA-062E:F	3200 MT/s	16	1	8	x8	1.09	1.63	1.06	1.51	1.03	1.37	1.01	1.17	4340	1916
S0	M378A2K43CB1-CTD	K4A8G085WC-BCTD	2666 MT/s	16	2	8	x8	1.04	3.21	1.03	2.63	1.01	2.33	1.00	1.27	12152	1965
S1	M393A1K43BB1-CTD	K4A8G085WB-BCTD	2666 MT/s	8	1	8	x8	1.04	1.85	1.01	1.83	1.00	1.79	1.00	1.41	31248	3326
S2	M378A1K43DB2-CTD	K4A8G085WD-BCTD	2666 MT/s	8	1	8	x8	1.05	1.85	1.03	1.67	1.01	1.49	1.00	1.13	6230	1664
S3	M471A4G43AB1-CWE	K4AAG085WA-BCWE	3200 MT/s	32	2	8	x8	1.05	1.60	1.03	1.48	1.01	1.37	1.00	1.14	8390	4355
S4	M471A5244CB0-CRC	Unknown ^a	2666 MT/s	4	1	4	x16	1.04	1.73	1.03	1.70	1.01	1.52	1.00	1.13	12418	1780
S5	M391A2G43BB2-CWE	Unknown ^a	3200 MT/s	16	1	8	x8	1.05	1.50	1.03	1.39	1.02	1.25	1.00	1.07	6685	2150
S6	M391A2G43BB2-CWE	Unknown ^a	3200 MT/s	16	1	8	x8	1.05	1.90	1.03	1.72	1.02	1.24	1.00	1.06	7575	3400
Chip0	Unknown ^a	Unknown ^a	460 GB/s	8	N/A	1	x2048	1.05	1.73	1.02	1.70	1.00	1.59	1.00	1.19	45136	1244
Chip1	Unknown ^a	Unknown ^a	460 GB/s	8	N/A	1	x2048	1.05	1.82	1.03	1.79	1.00	1.71	1.00	1.37	41664	2218
Chip2	Unknown ^a	Unknown ^a	460 GB/s	8	N/A	1	x2048	1.05	1.72	1.02	1.52	1.00	1.32	1.00	1.09	34720	1520
Chip3	Unknown ^a	Unknown ^a	460 GB/s	8	N/A	1	x2048	1.05	1.89	1.02	1.83	1.00	1.73	1.00	1.23	55553	1664

^aUnknown indicates that the module or chip identifier is not discernible by visual inspection of the DDR4 module or the HBM2 chip.

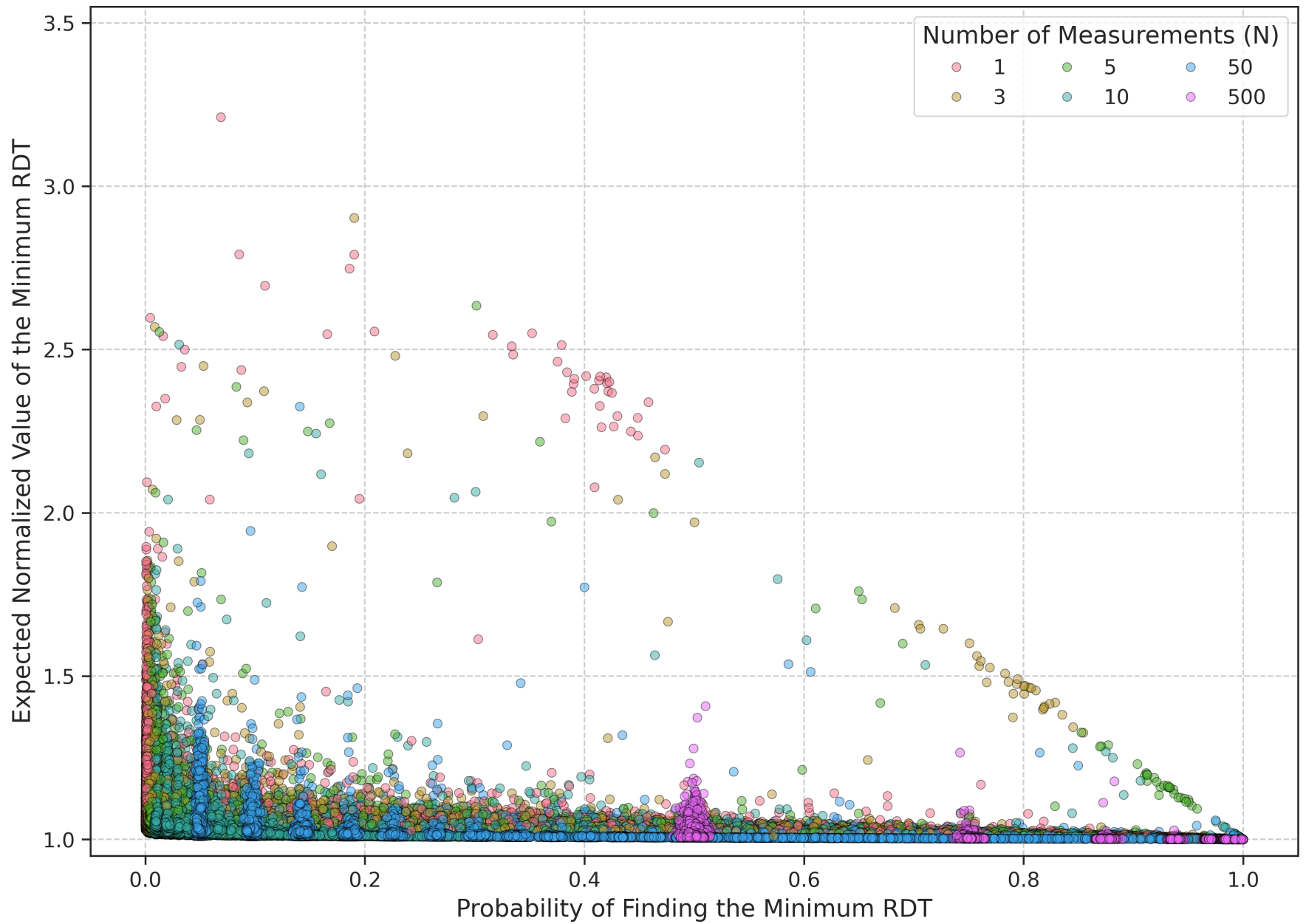


Figure 25: Large and expanded version of the bottom plot in Fig. 8: the expected normalized value of the minimum RDT over the probability of finding the minimum RDT